Quantum dots and Nanoparticles for Biological Application

- Chapter 22
- Chapter 23

II - VI

GaAs

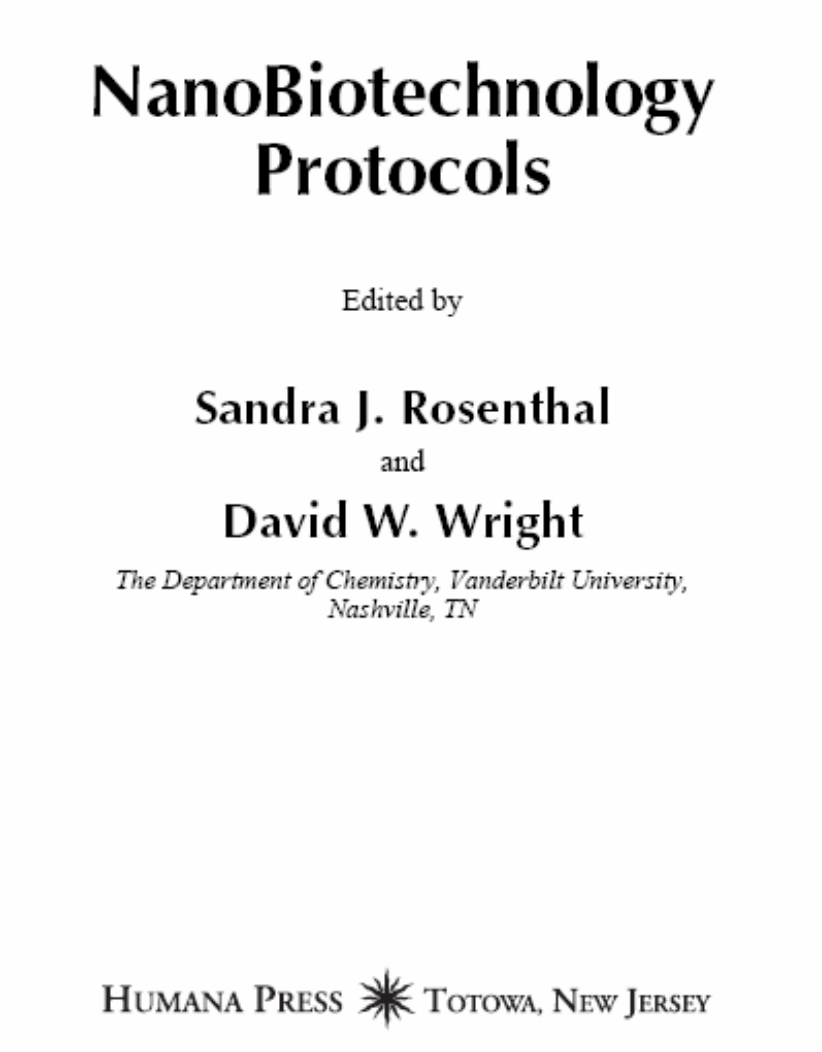

Applications of Quantum Dots in Biology

An Overview

Charles Z. Hotz

- Size dependent emission spectra
- Single excitation
- Higher photostability
- Narrow emission peak
- Low toxicity for coated quantum dots

Nucleation and Growth of CdSe on ZnS Quantum Crystallite Seeds, and Vice Versa, in Inverse Micelle Media

A. R. Kortan, R. Hull, R. L. Opila, M. G. Bawendi, M. L. Steigerwald, P. J. Carroll, and L. E. Brus*

Contribution from AT&T Bell Laboratories, Murray Hill, New Jersey 07974.
Received June 20, 1989

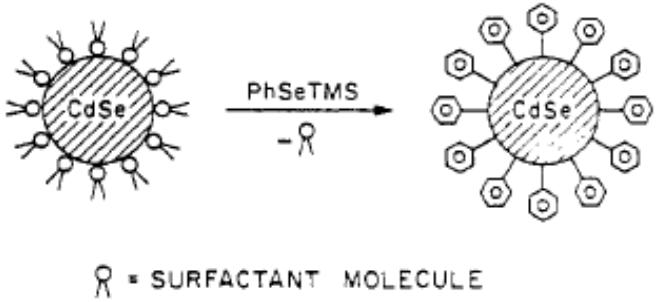

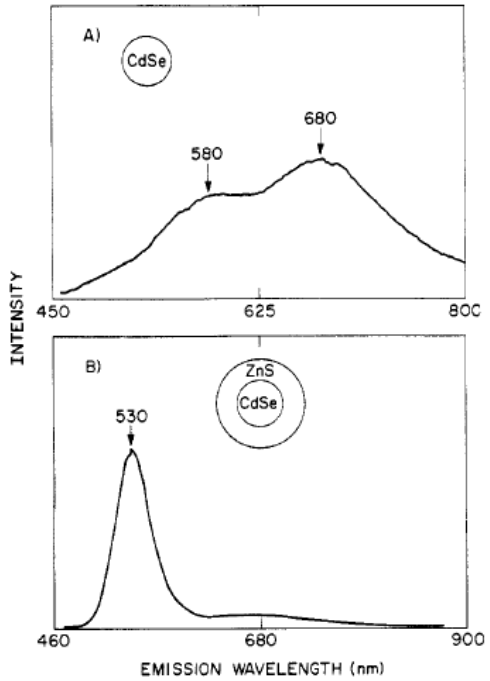

Figure 2. Room temperature luminescence spectra after annealing: (A) (CdSe)Ph, (B) $(CdSe)_1(ZnS)_4Ph$. The integrated quantum yield in B is more than an order of magnitude higher than in A.

Semiconductor Nanocrystals as Fluorescent Biological Labels

Marcel Bruchez Jr., Mario Moronne, Peter Gin, Shimon Weiss,*
A. Paul Alivisatos*

SCIENCE VOL 281 25 SEPTEMBER 1998

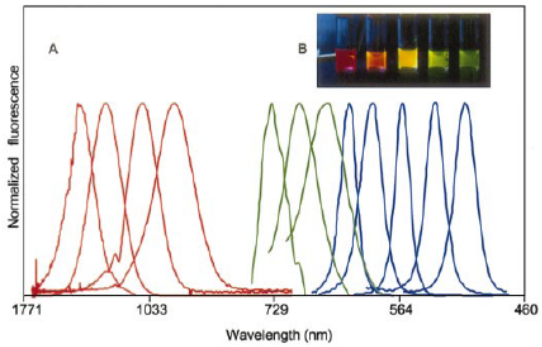

Fig. 2. (**A**) Size- and material-dependent emission spectra of several surfactant-coated semiconductor nanocrystals in a variety of sizes. The blue series represents different sizes of CdSe nanocrystals (*16*) with diameters of 2.1, 2.4, 3.1, 3.6, and 4.6 nm (from right to left). The green series is of InP nanocrystals (*26*) with diameters of 3.0, 3.5, and 4.6 nm. The red series is of InAs nanocrystals (*16*) with diameters of 2.8, 3.6, 4.6, and 6.0 nm. (**B**) A true-color image of a series of silica-coated core (CdSe)–shell (ZnS or CdS) nanocrystal probes in aqueous buffer, all illuminated simultaneously with a handheld ultraviolet lamp.

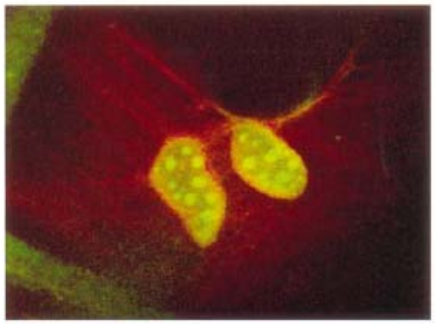

Fig. 3. Cross section of a dual-labeled sample examined with a Bio-Rad 1024 MRC laser-scanning confocal microscope with a 40× oil 1.3 numerical aperture objective. The mouse 3T3 fibroblasts were grown and prepared as described in (*27*). A false-colored image was obtained with 363-nm excitation, with simultaneous two-channel detection (522DF 35-nm FWHM narrow-pass filter for the green, and a 585-nm long-pass filter for the red). Image width: 84 μm.

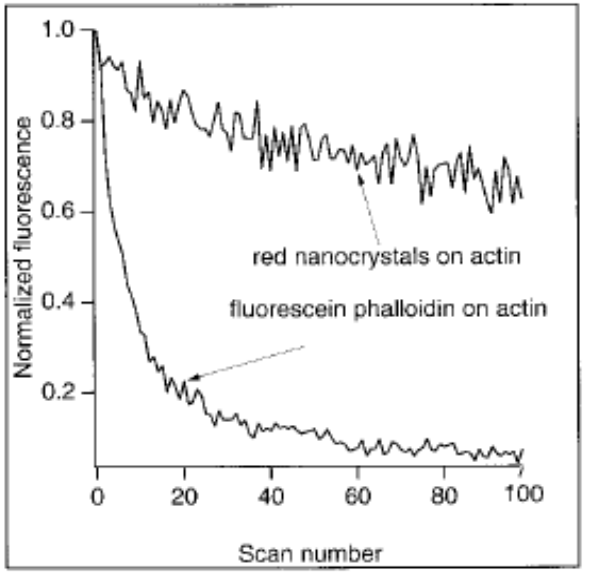

Fig. 4. Sequential scan photostability comparison of fluorescein-phalloidin–labeled actin fibers compared with nanocrystal-labeled actin fibers. Fluorescein was excited at 488 nm and the nanocrystals at 363 nm by a laser scanning confocal microscope with a 12-μs dwell time and ~20-mW power for each laser. The average intensity of four pixels was followed in each sample through 100 successive scans and normalized to its initial value. The intensity of the fluorescein drops quickly to autofluorescence levels, whereas the intensity of the nanocrystals drops only slightly.

Quantum Dot Bioconjugates for Ultrasensitive Nonisotopic Detection

Warren C. W. Chan and Shuming Nie*

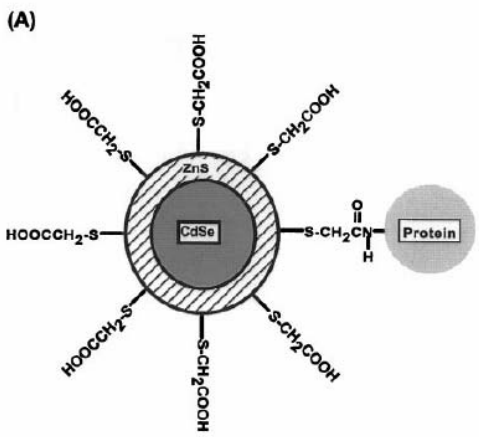

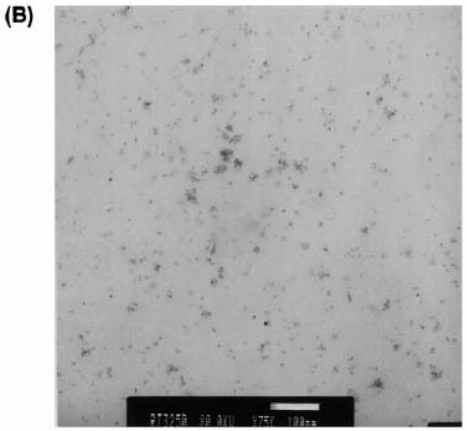

Fig. 1. (**A**) Schematic of a ZnS-capped CdSe QD that is covalently coupled to a protein by mercaptoacetic acid. (**B**) TEM of QD-transferrin (an iron-transport protein) conjugates. Scale bar, 100 nm. Clusters of closely spaced particles were mainly formed by sample spreading and drying on the carbon grid and not by chemical cross-linking. ZnS-capped QDs with a CdSe core size of 4.2 nm were prepared according to the procedure developed by Hines and Guyot-Sionnest (*7*). The colloidal QDs were dissolved in chloroform and were reacted with glacial mercaptoacetic acid (~1.0 M) for 2 hours. An aqueous phosphate-buffered saline (PBS) solution (pH 7.4) was added to this reaction mixture at a 1:1 volume ratio. After vigorous shaking and mixing, the chloroform and water layers separated spontaneously. The aqueous layer, which contained mercapto-coated QDs, was extracted. Excess mercaptoacetic acid was removed by four or more rounds of centrifugation. The purified QDs were conjugated to transferrin and IgG with the cross-linking reagent ethyl-3-(dimethylaminopropyl)carbodiimide. Standard protocols were followed (*16*), except the excess proteins were removed by repeated centrifugation. The purified conjugates were stored in PBS at room temperature.

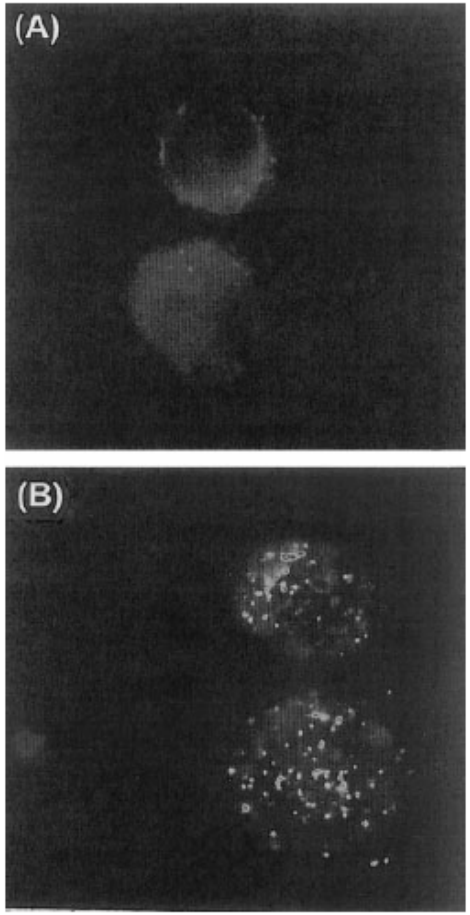

Fig. 4. Luminescence images of cultured HeLa cells that were incubated with (**A**) mercapto-QDs and (**B**) QD-transferrin conjugates. The QD bioconjugates were transported into the cell by receptor-mediated endocytosis and were detected as clusters or aggregates. Luminescence "blinking" was not observed for these clusters because of statistical averaging. The images were obtained with an epifluorescence microscope that was equipped with a high-resolution CCD camera (1.4 million pixels) (Photometrix, Tucson, Arizona) and a 100-W Hg excitation lamp. HeLa cells were grown in a minimum essential medium containing 10% fetal calf serum, 1% antibiotics (penicillin and streptomycin), and fungizone. The cultured cells were incubated overnight with either control QDs or the transferrin conjugates at 37°C. After repeated washings to eliminate excess QDs, the cells were removed from the petri dish and placed on a glass cover slip for imaging. The trypsin-treated cells had a spherical shape on the cover slip. Cell diameter, ~10 μm.

Optical Properties

- Broadband Absorption
  - Single laser excitation
- Sharp Emission
  - 20-30 nm symmetric emission
- High Quantum Yield
  - 20 x more than R6G
- Good Photostability
  - 100 x more stable for R6G (4 Hrs vs 10 mins)
- Longer fluorescent lifetime (20-40 ns vs 5 ns)

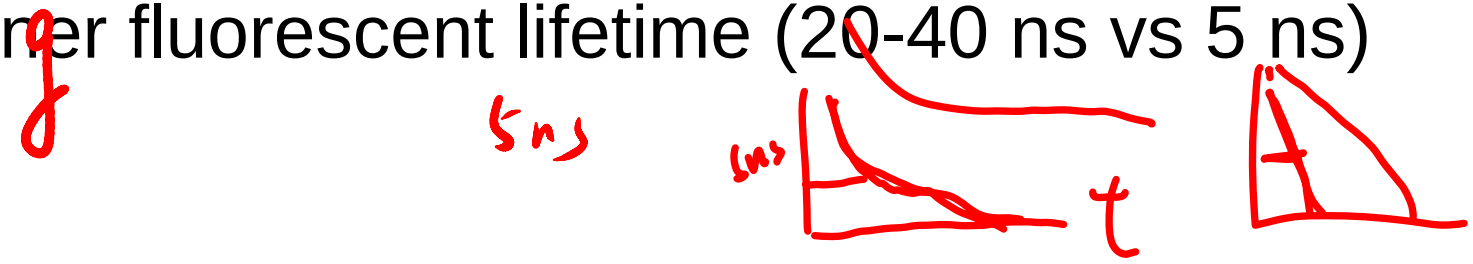

Structure

- Core quantum dot
  - CdSe, hydrophobic, not stable, lower QE (~5%)
  - Defects =>Trap state
- Core-shell quantum dot
  - ZnS/CdSe, hydrophobic, stable, higher QE (~50%)
  - Coated with higher bandgap materials or passivation reduces defects
- Water soluble quantum dot
  - Hydrophilic polymer coating
- Quantum dot bioconjugation
  - Bioconjugate to hydrophilic quantum dot

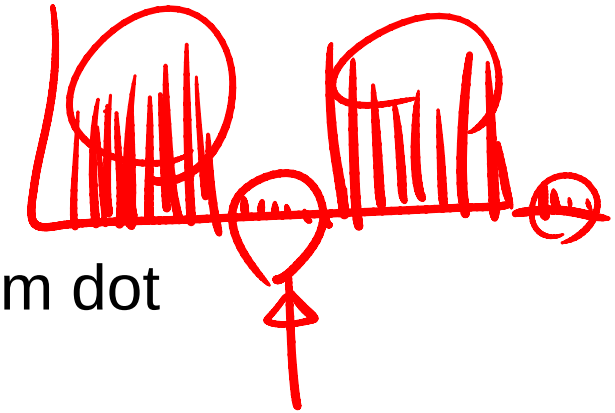

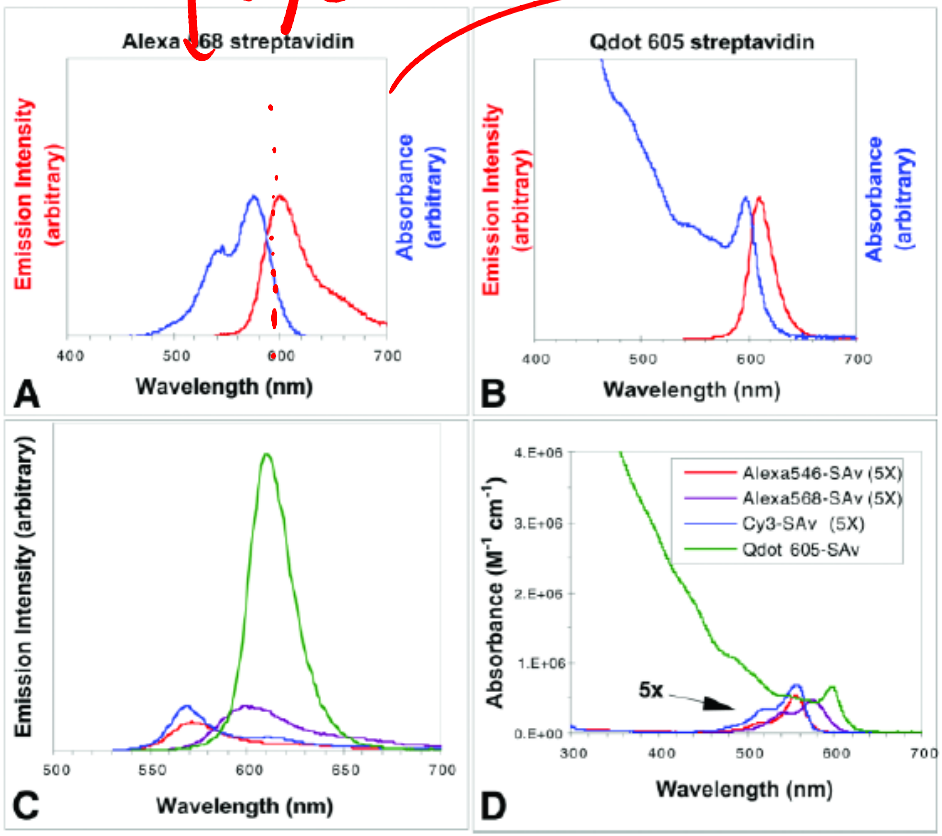

Fig. 1. Comparison of absorbance and emission spectra (normalized) of **(A)** Alexa® 568 streptavidin conjugate and **(B)** Qdot® 605 streptavidin conjugate. Note that the quantum dot conjugate can absorb light efficiently far to the blue of the emission. **(C)** Comparison of emission spectra (nonnormalized) of streptavidin conjugates of Qdot 605 (—), Alexa 546 (—), Alexa 568 (—), and Cy3® (—). The spectra were taken under conditions in which each fluorophore absorbed the same amount of excitation light. The measured quantum yields of the conjugates were 55, 8, 16, and 11%, respectively. **(D)** Comparison of absorbance spectra (nonnormalized, each 1 μ*M* flurophore) of Qdot 605 streptavidin conjugate (—), Cy3 streptavidin conjugate (—), Alexa 546 streptavidin conjugate (—), and Alexa 568 streptavidin conjugate (—). Note that all dye spectra are enhanced fivefold for clarity. Alexa, Cy3, and Qdot are registered trademarks of Molecular Probes, Amersham Biosciences, and Quantum Dot Corporation, respectively.

Table 1
Optical Properties of Quantum Dots Compared to Common Dyes[a]

Fluorescent dye	$\lambda_{excitation}$ (nm)	$\lambda_{emission}$ (nm)	ε(mol^{-1}-cm^{-1})
Qdot 525	400	525	280,000
Alexa 488	495	519	78,000
Fluorescein	494	518	79,000
Qdot 565	400	565	960,000
Cy3	550	570	130,000
Alexa 555	555	565	112,000
Qdot 585	400	585	1,840,000
R-Phycoerythrin	565	578	1,960,000
TMR	555	580	90,000
Qdot 605	400	605	2,320,000
Alexa 568	578	603	88,000
Texas Red	595	615	96,000
Qdot 655	400	655	4,720,000
APC	650	660	700,000
Alexa 647	650	668	250,000
Cy5	649	670	200,000
Alexa 647-PE	565	668	1,960,000

[a]The extinction coefficients (ε) are generally much larger for quantum dots than for fluorescent dyes. Furthermore, the excitation wavelength ($\lambda_{excitation}$) can be much farther from the emission ($\lambda_{emission}$).

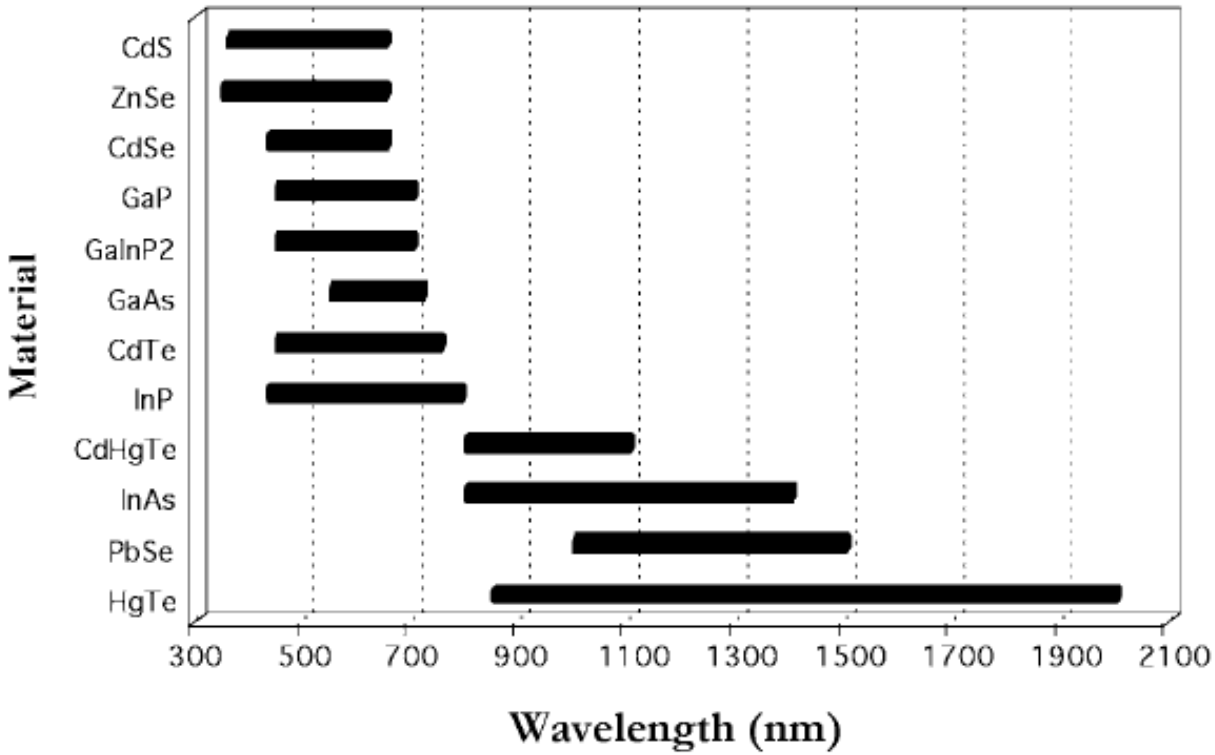

Fig. 5. Wavelength ranges obtainable by varying size of quantum dots made from a number of different semiconductor materials. Each bar approximately represents the range of wavelengths obtained from the smallest (left end) to largest (right end) quantum dot made from the material listed.

Photo Stability

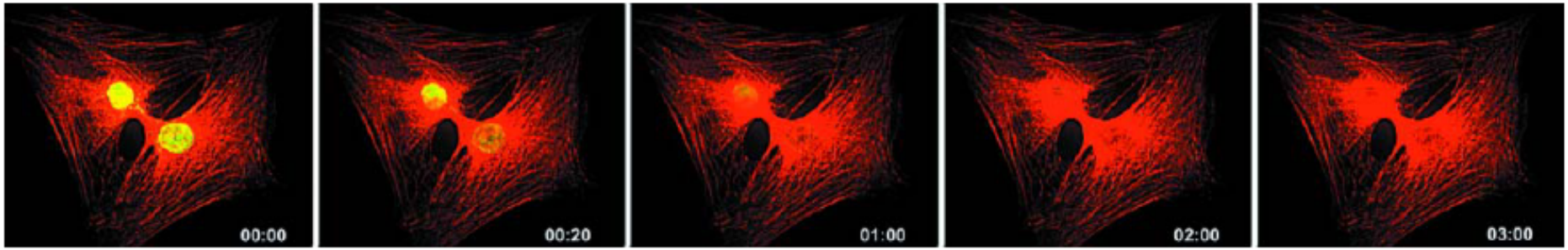

Fig. 2. Comparison of photostability between Qdot® 605 and Alexa Fluor® 488 streptavidin conjugates. Actin filaments in two 3T3 mouse fibroblast cells were labeled with Qdot 605 streptavidin conjugate (red), and the nuclei were stained with Alexa Fluor 488 streptavidin (green). The specimens were continuously illuminated for 3 min with light from a 100-W mercury lamp under a ×100 1.30 oil objective. An excitation filter (excitation: 485 ± 20 nm) was used to excite both Alexa 488 and Qdot 605. Emission filters (emission: 535 ± 10 and em 605 ± 10 nm) on a motorized filter wheel were used to collect Alexa 488 and Qdot 605 signals, respectively. Images were captured with a cooled charge-coupled device camera at 10-s intervals for each color automatically. Images at 0, 20, 60, 120, and 180 s are shown. Whereas Alexa 488 labeling signal faded quickly and became undetectable within 2 min, the Qdot 605 signal showed no obvious change for the entire 3-min illumination period.

Size of Quantum dots

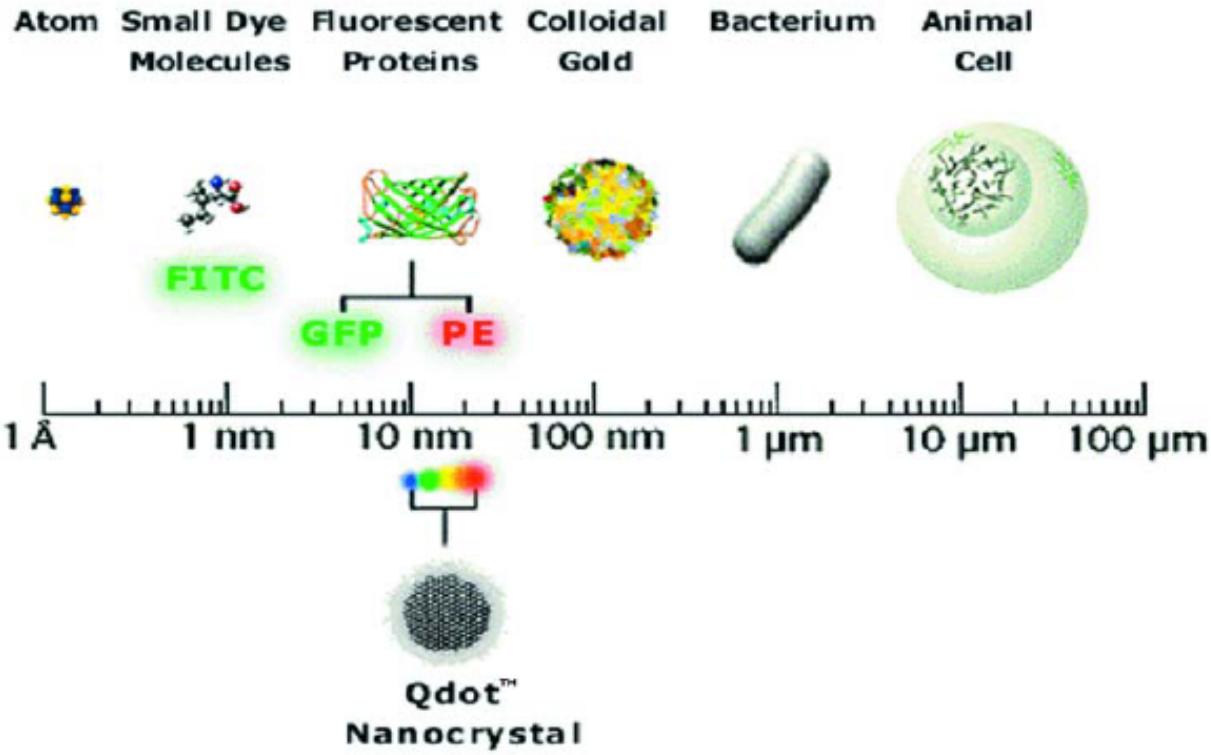

Fig. 4. Physical size of quantum dots compared to related entities.

Surface Modification

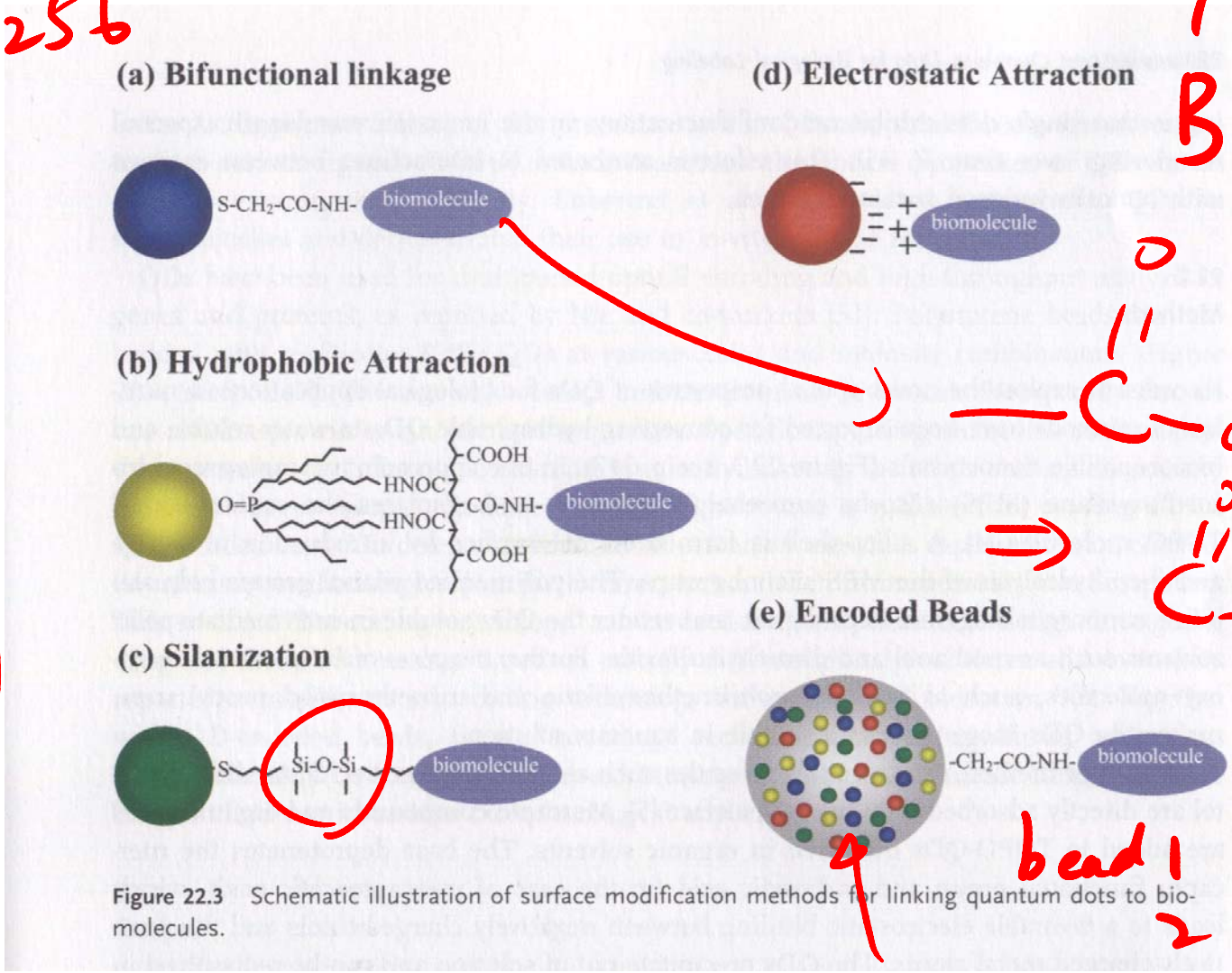

Figure 22.3 Schematic illustration of surface modification methods for linking quantum dots to biomolecules.

Q-dot labeling Schemes

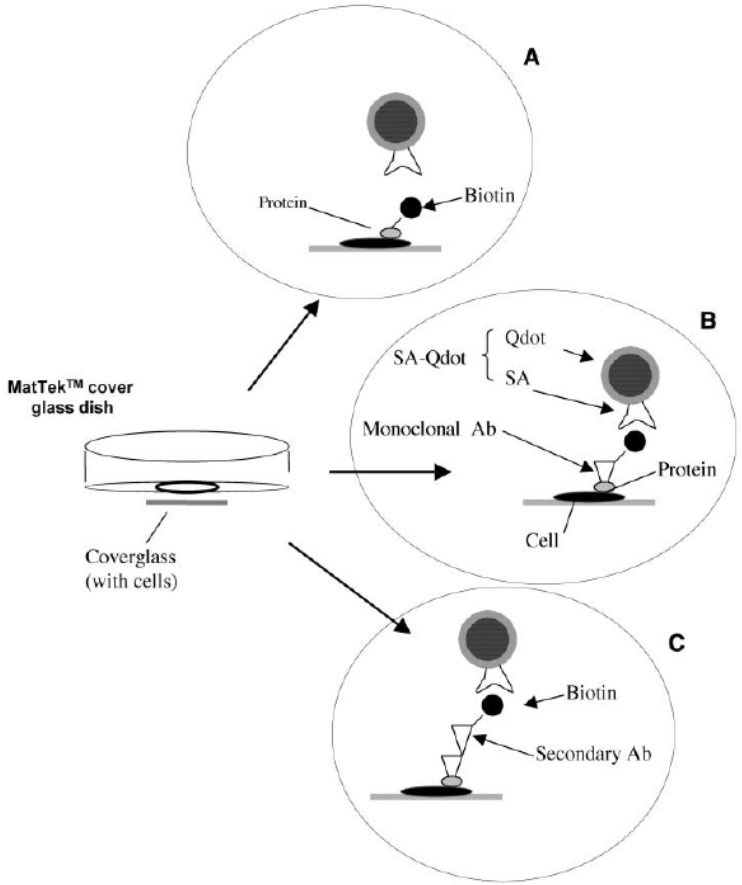

Fig. 3. Direct and indirect labeling of live cells by SA-quantum dots (SA-Qdot). **(A)** Biotinylated cell-surface proteins are labeled directly by SA-quantum dots. **(B)** Biotinylated MAb used to detect cell-surface protein is labeled by SA-quantum dots. **(C)** Biotinylated secondary antibody used to detect polyclonal antibody attached to the cell-surface protein is labeled by SA-quantum dot.

Biotinylation

Biotin is very easy to attach to most biomolecules, and then to detect. This 244Da vitamin binds with one of the highest affinity amongst biomolecules, to both avidin ($Ka=10^{-15}$ M^{-1}) and streptavidin ($Ka=10^{-14}$ M^{-1}).
This is taken to advantage in detection and separation techniques

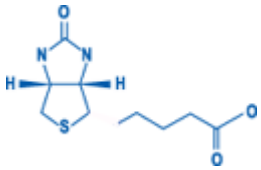

Biotin

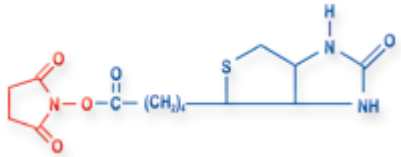

NHS-Biotin

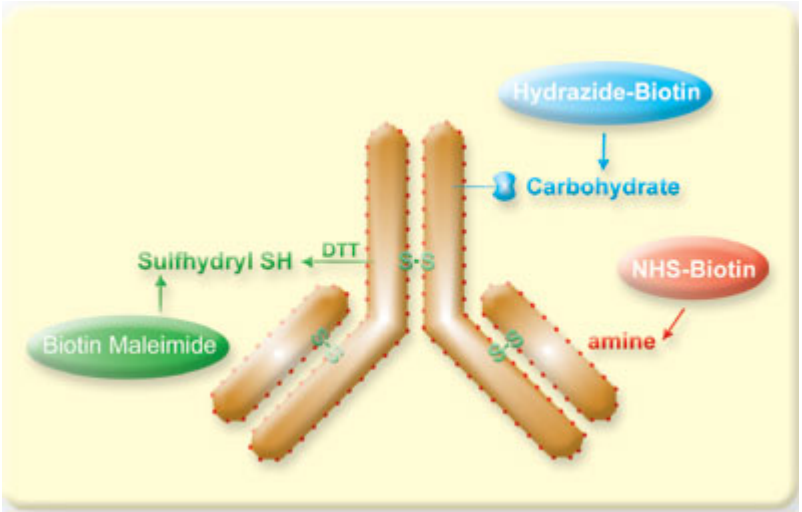

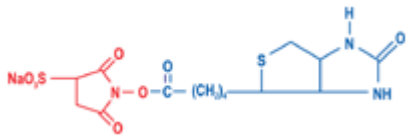

SulfoNHS-Biotin

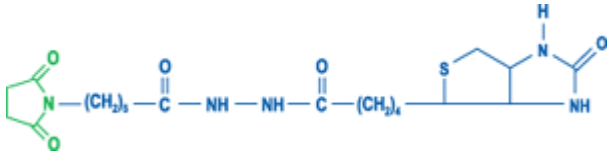

Maleimido-Biotin

Biotin Labeling

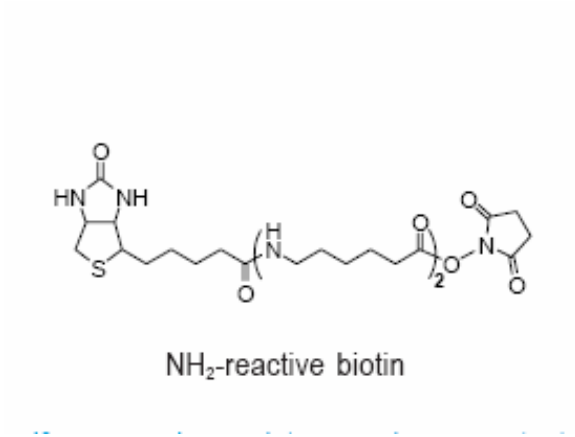

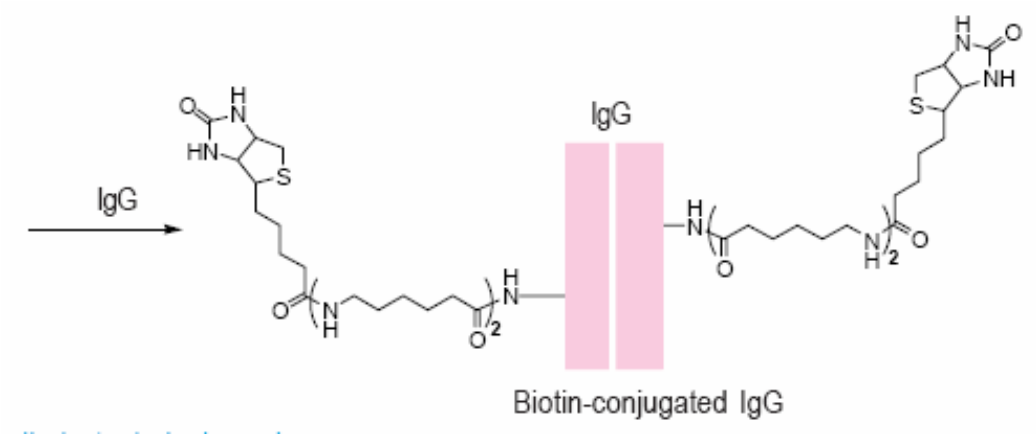

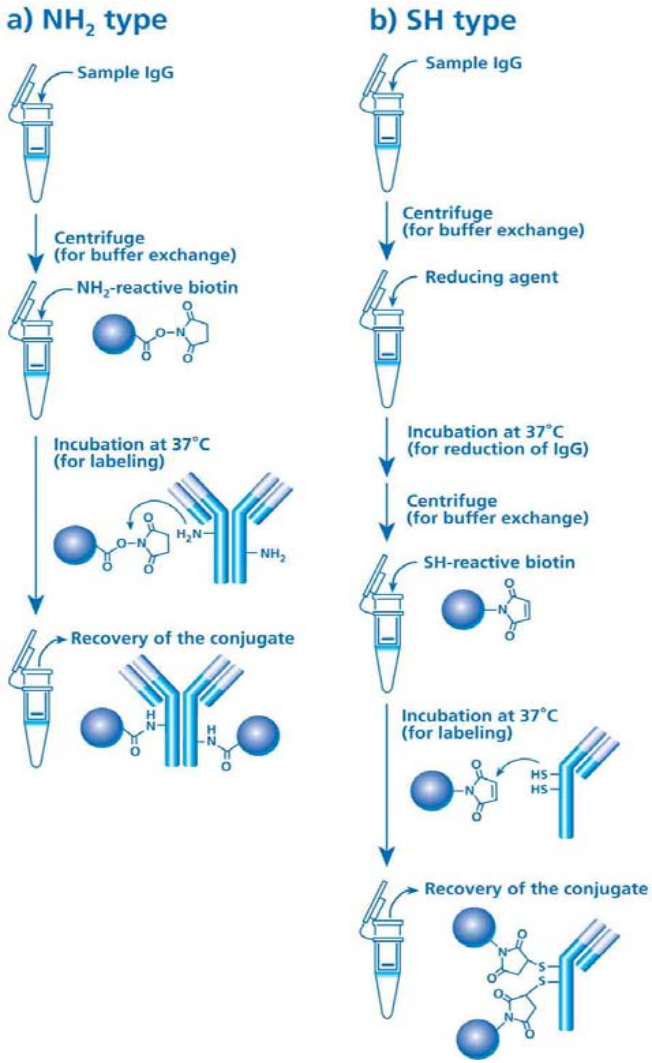

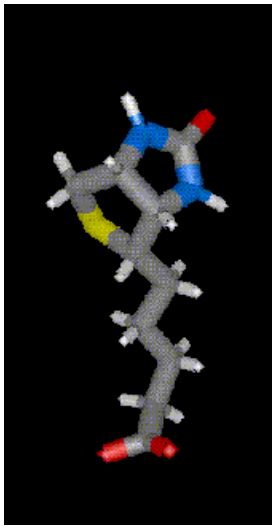

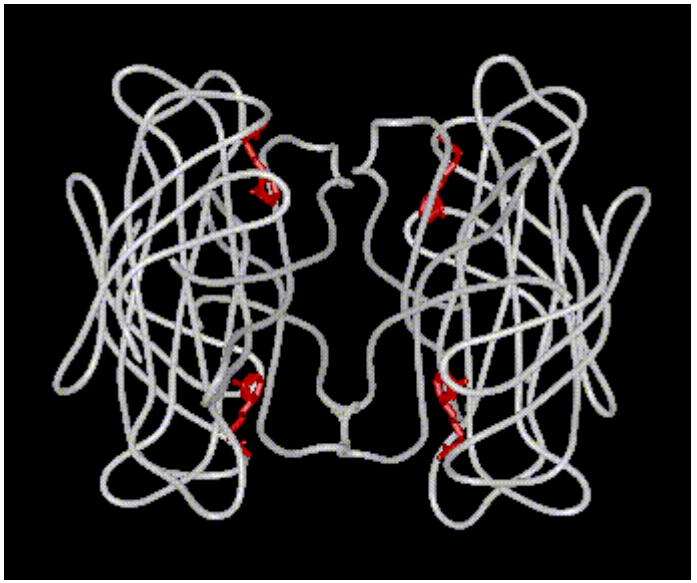

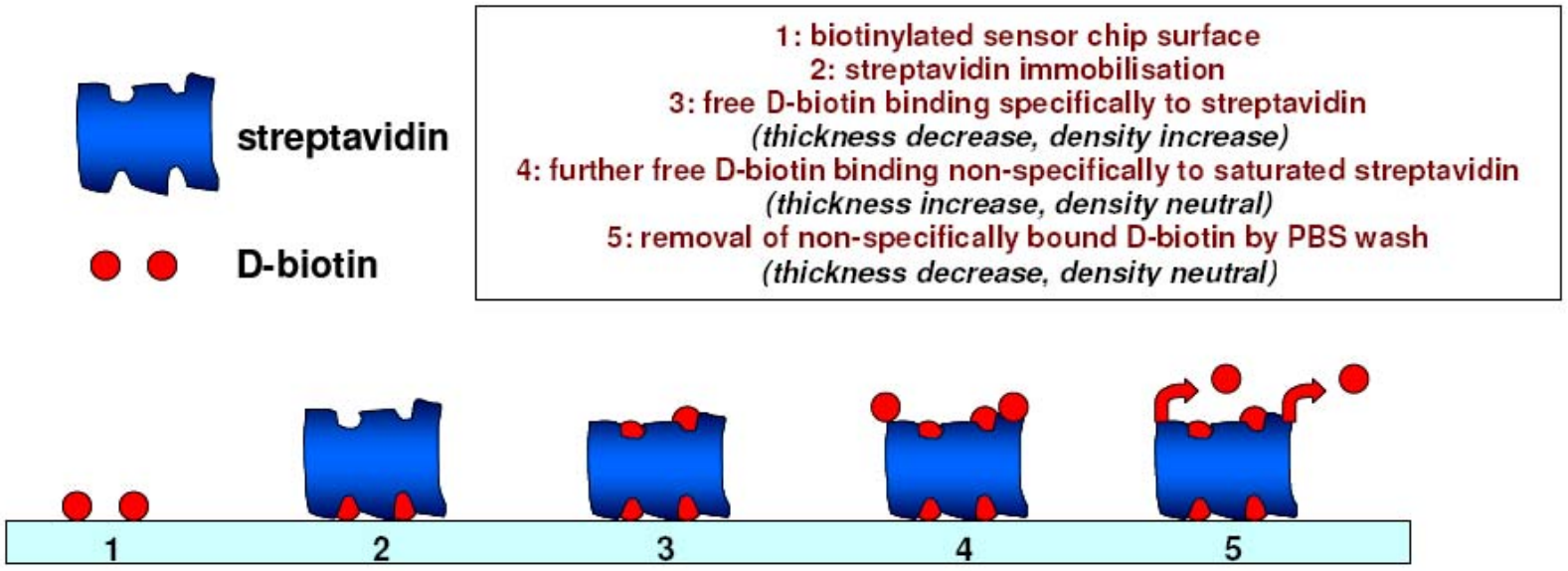

Figure 3: Visual schematic of D-biotin-streptavidin interactions

Multicolor Labeling

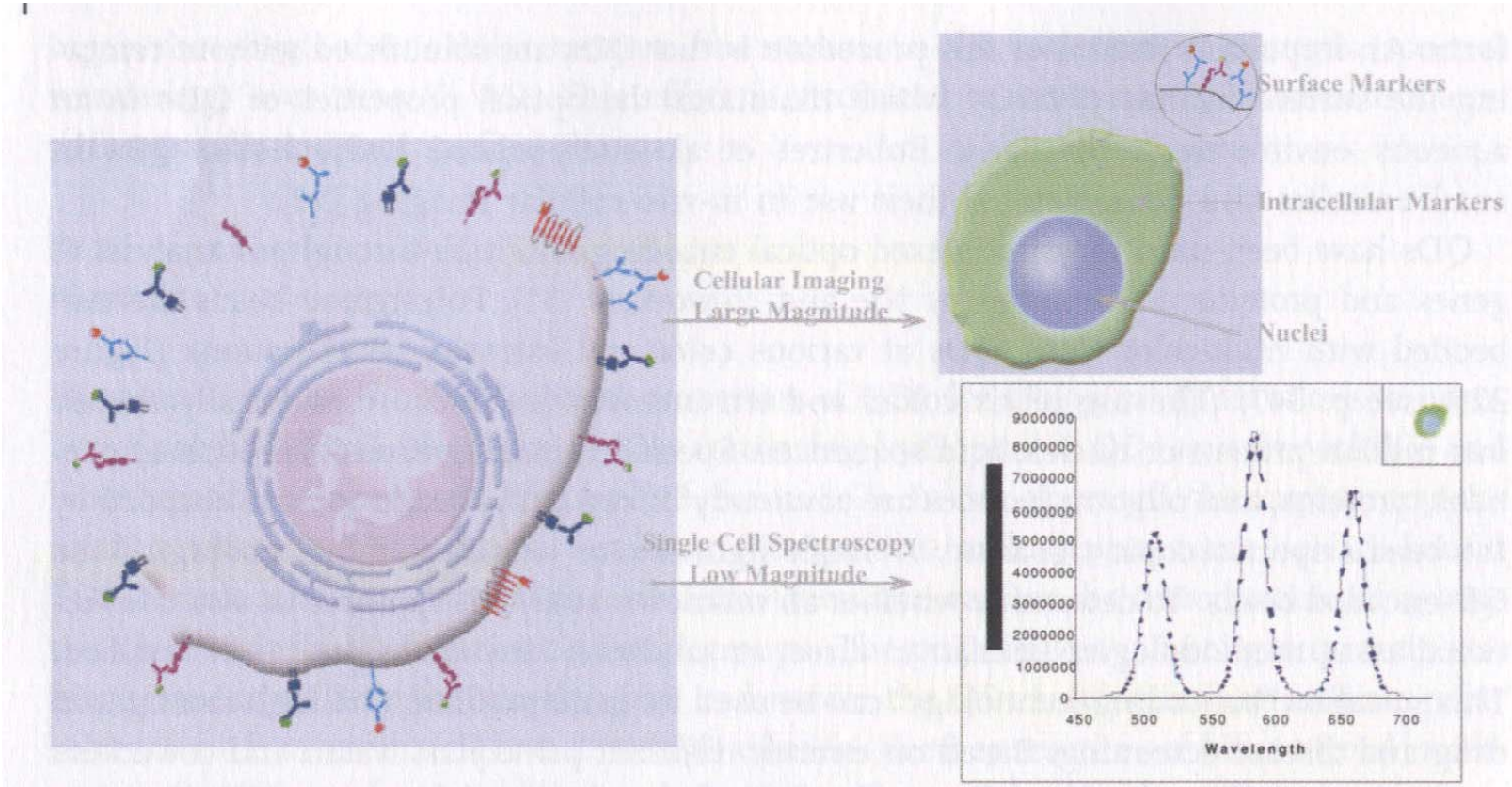

Figure 22.5 Schematic illustration of cell staining using biomolecules attached with multicolor QDs. Small color particles represent bioconjugated quantum dots.

Encoding

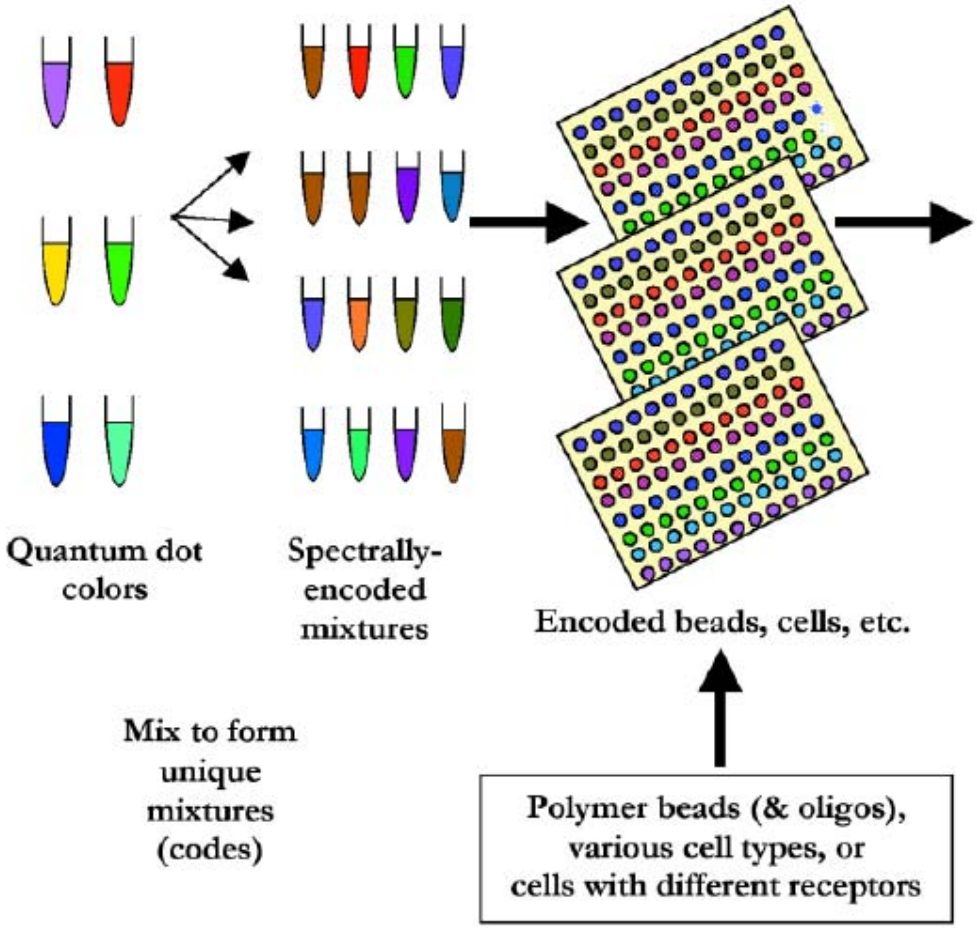

Application	Format
Multiplexed gene expression	Encoded beads each with gene-specific oligos
Multiplexed SNP genotyping	Encoded beads with allele-specific oligos
Multiplexed immunoassays	Encoded beads with antibodies
Multiplexed cell-based assays	Mixed cell types encoded with quantum dots
Multiplexed reporter assays	Encoded cell lines expressing various receptors

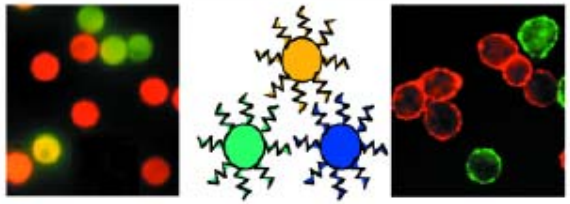

Fig. 6. Concept of encoding using quantum dots. Quantum dot colors can be mixed to produce spectral codes. These mixtures can be combined with polymer beads to produce encoded beads that can be subsequently coupled to distinct oligonucleotides or other affinity molecules. Alternatively, the quantum dot spectral codes can be used to label cells to differentiate cell lines, or cell lines bearing different receptors. SNP, single nucleotide polymorphism.

Labeling Cell-Surface Proteins Via Antibody Quantum Dot Streptavidin Conjugates

John N. Mason, Ian D. Tomlinson, Sandra J. Rosenthal,
and Randy D. Blakely

Cell Culture

In the remainder of this section, each step was performed using aseptic technique inside a laminar flow hood (*see* **Note 2**). Ten milliliters of medium was transferred by pipet into each labeled flask. Thawed vials were then sterilized by swabbing with alcohol. The vials were slowly opened, and the medium with the cells was transferred by pipet into the appropriately labeled flask. The flasks were next placed in a 37°C incubator at 5% CO_2, and the cells were allowed to grow until confluent.

Once confluent, the medium was aspirated off and the cells well rinsed with PBS, and then 3 mL of 0.1% trypsin was added. After approx 1 to 2 min, or when the cells began to round up and detach, 3 mL of medium was added to disperse the cells and to inhibit the trypsin (*see* **Note 3**). Cells from each flask were then transferred to an appropriately labeled 50-mL conical tube and centrifuged at 500*g* for 5 min. The supernatant was aspirated off, and the cells were resuspended in fresh medium.

Using a hemacytometer, the cells were counted and their concentration was determined (*see* **Note 4**). The cell solution was next diluted to 1×10^5 cells/mL and 150 µL was added to the glass cover slip of poly-D-lysine coated sterile MatTek microwell dishes. The cells were incubated at 37°C with 5% CO_2 for 3 h to allow the cells to attach. Once the cells had attached, 2 mL of additional medium was added to the dish. The dishes were then returned to the incubator and allowed to grow for 3 d or until 50% confluent.

Hemacytometer

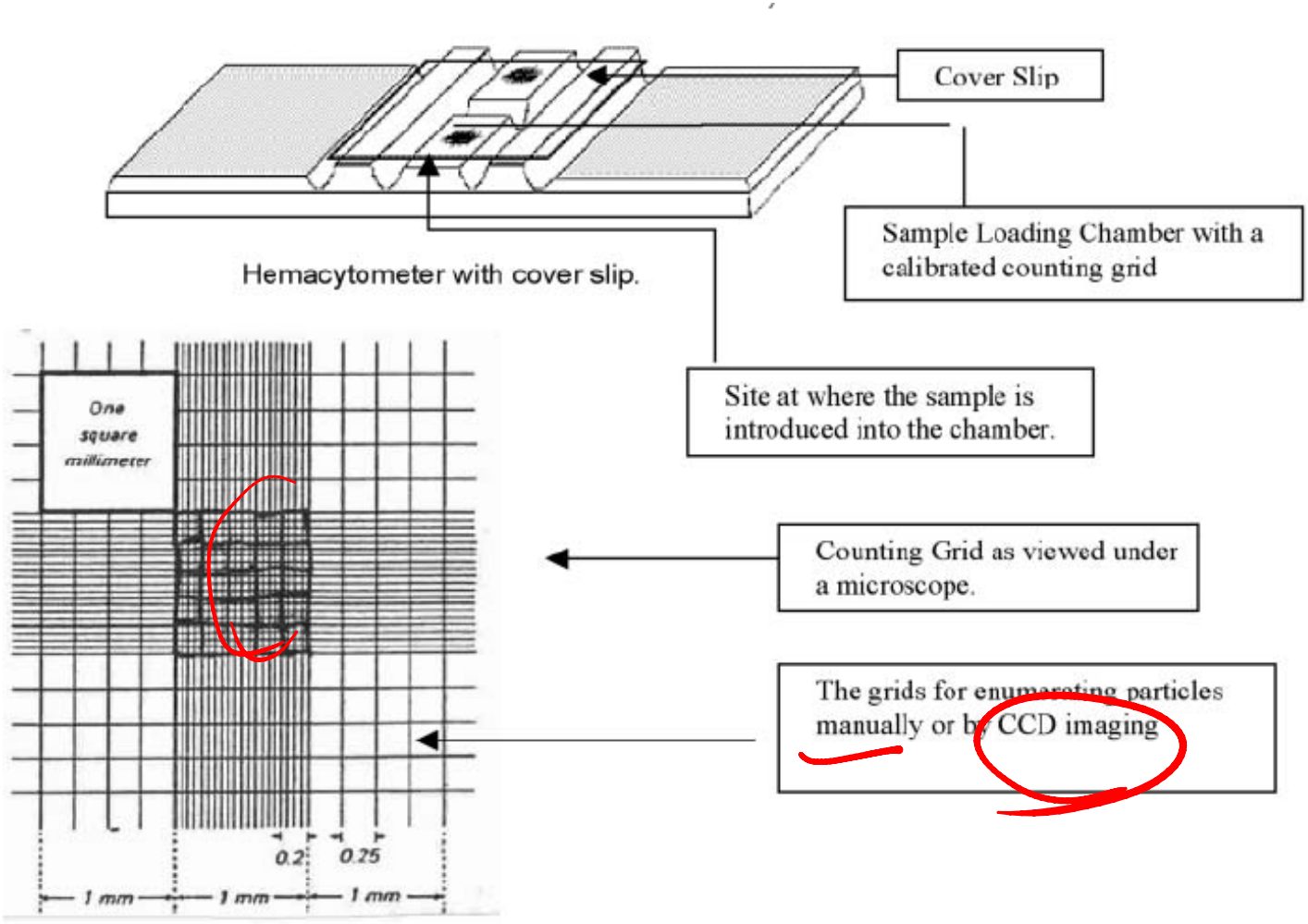

Fig. 3. Layout of hemacytometer.

Fluorescence Imaging Scheme

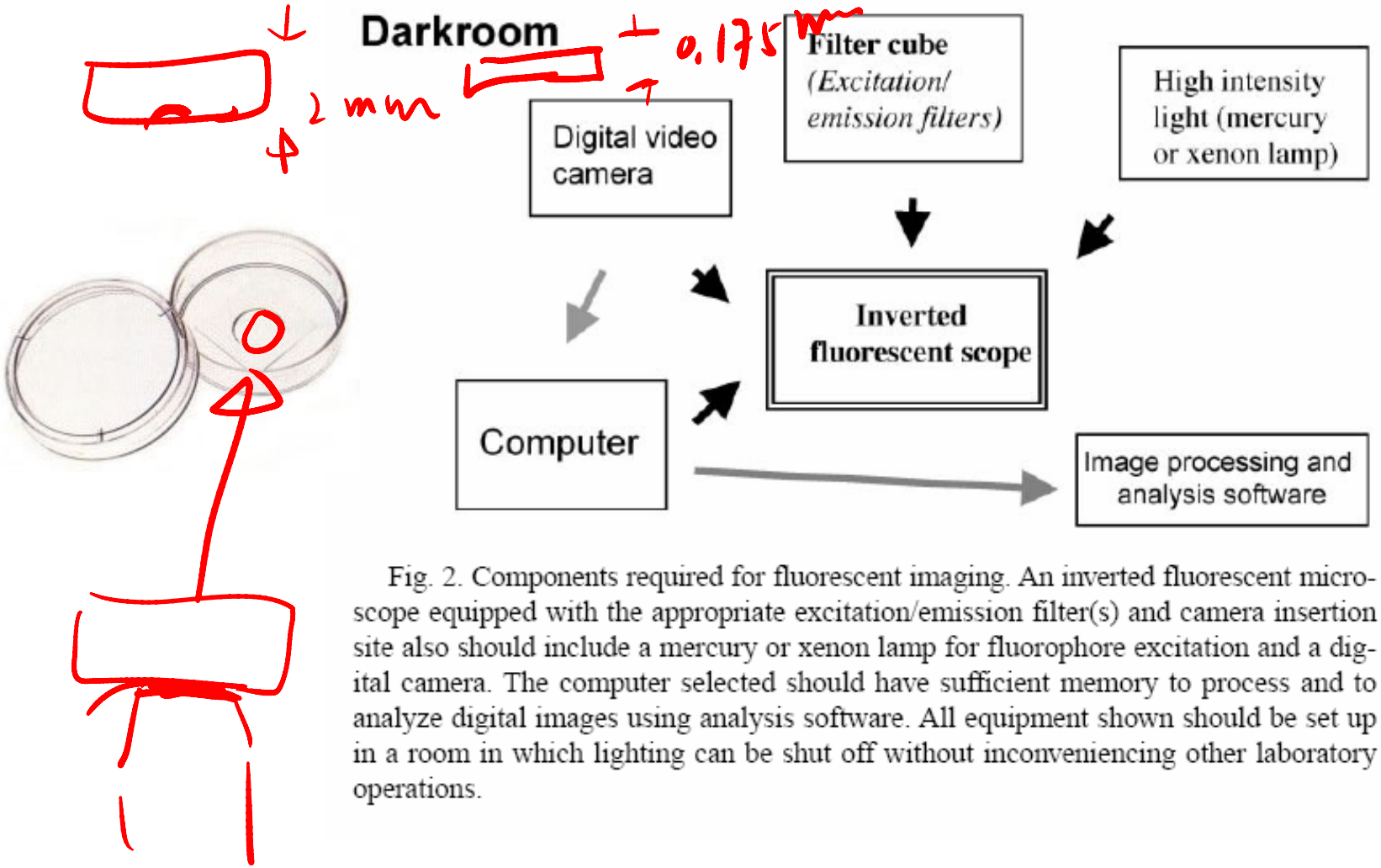

Fig. 2. Components required for fluorescent imaging. An inverted fluorescent microscope equipped with the appropriate excitation/emission filter(s) and camera insertion site also should include a mercury or xenon lamp for fluorophore excitation and a digital camera. The computer selected should have sufficient memory to process and to analyze digital images using analysis software. All equipment shown should be set up in a room in which lighting can be shut off without inconveniencing other laboratory operations.

Quantum Dot Bio-conjugation

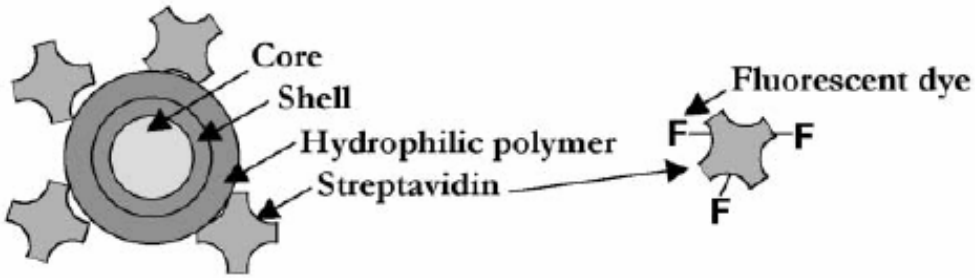

Fig. 3. Schematic of Qdot™ Nanocrystal Probe compared to a typically labeled fluorescent dye protein conjugate (see text for descriptions). Proteins generally carry several fluorescent dye labels (F). By contrast, each quantum dot is conjugated to multiple protein molecules.

Q-dot Aggregation

Clustering

Clustering

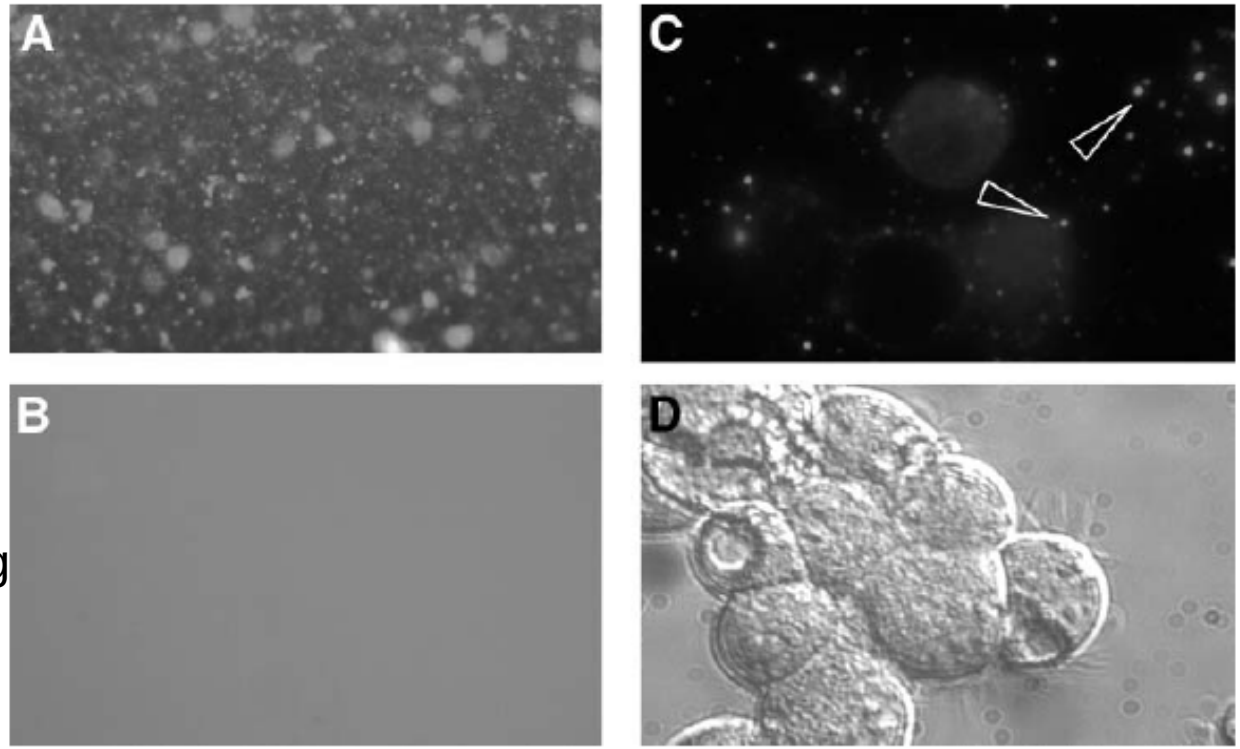

Non-Clustering

Fig. 4. Evidence for quantum dot aggregation (magnification: ×40): **(A)** fluorescent image of aggregated SA-quantum dots in absence of cells; **(B)** image of nonaggregated SA-quantum dots in absence of cells; **(C)** image of cells surrounded by aggregated SA-quantum dots (arrowheads); **(D)** bright-field image.

Biotinylated Cell

Cell + Biotin

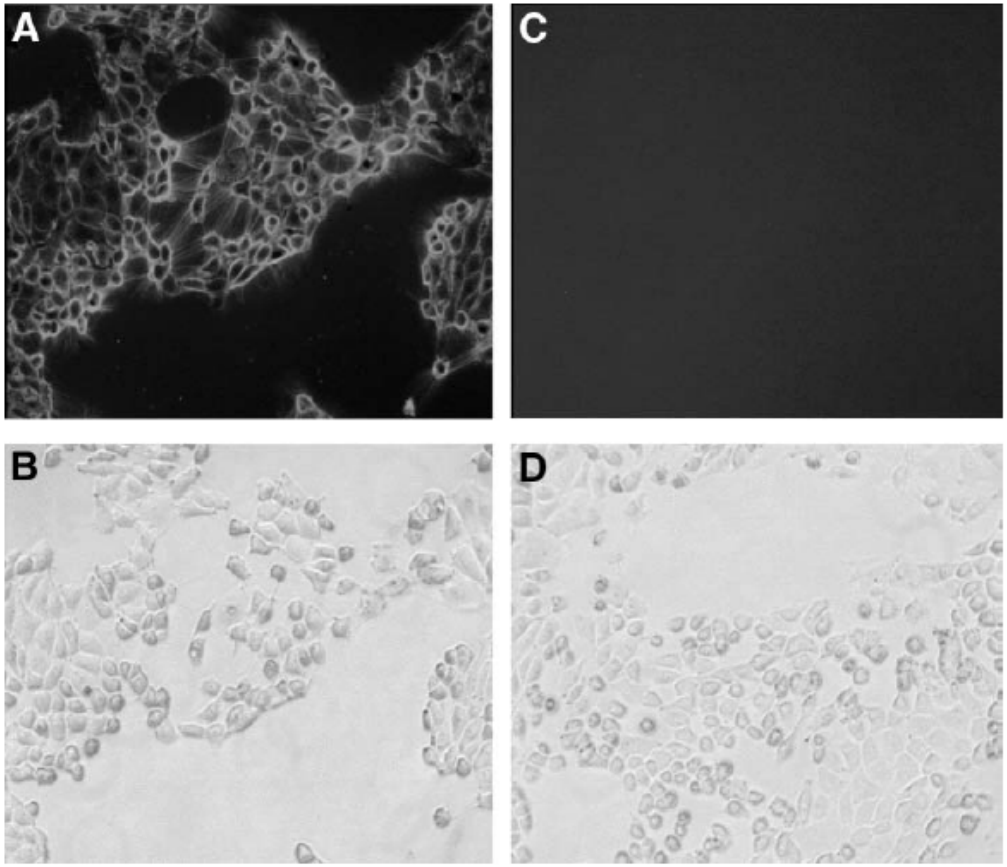

Fig. 1. Labeling of biotinylated HEK293 cells with SA-quantum dots (magnification: ×10). Three-day-old HEK293 cells cultured on poly-D-lysine glass-bottomed microwell dishes were biotinylated as described in **Subheading 3.2.1.** **(A,B)** Biotinylated HEK293 cells incubated with SA-quantum dots (50 n*M*); **(C,D)** biotinylated HEK293 cells labeled with SA-quantum dots after preincubating with 2 mg/mL of biotin.

Q-dot Antibody Labeling

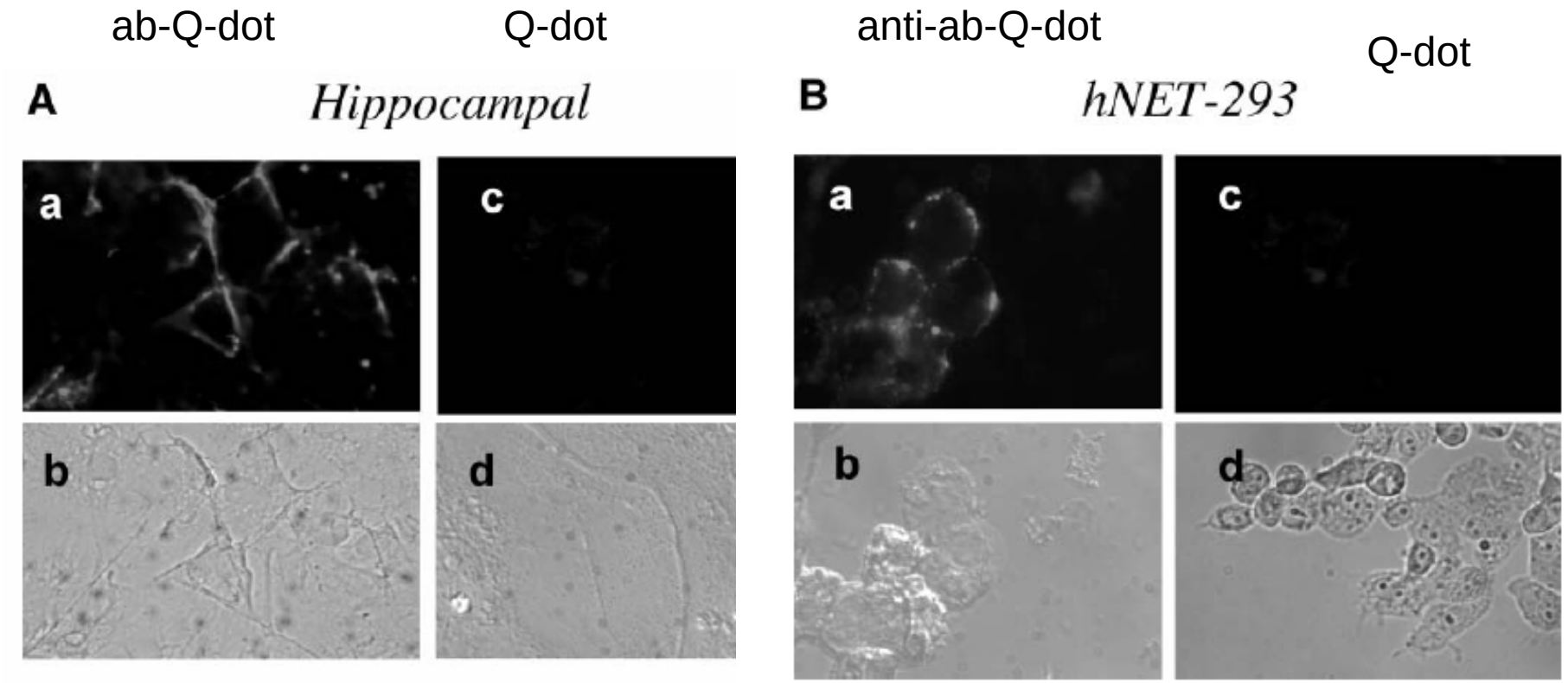

Fig. 5. SA-quantum dots and SA-Alexa Red recognize biotin-modified antibody-labeled cultures. **(A)** Eight-day-old *fixed* primary hippocampal cultures incubated with anti-LAMP followed by SA-quantum dots (a, b) or SA-quantum dots alone (c, d); **(B)** labeling of live hNET-293 cells with anti-hNET + biotinylated anti-rabbit IgG followed by SA-quantum dots (a, b) or SA-quantum dots alone (c, d).

Peptide-Conjugated Quantum Dots

Imaging the Angiotensin Type 1 Receptor in Living Cells

Ian D. Tomlinson, John N. Mason, Randy D. Blakely,
and Sandra J. Rosenthal

Peptide Angiotensin II (AnG II) ➔
mPEG-Amine-Conjugated AMP coated CdSe/ZnS

Cell lines:

1) CHO cell parental line
2) CHO cell expressing Ang II receptor

Ang II Labeled Q-dot

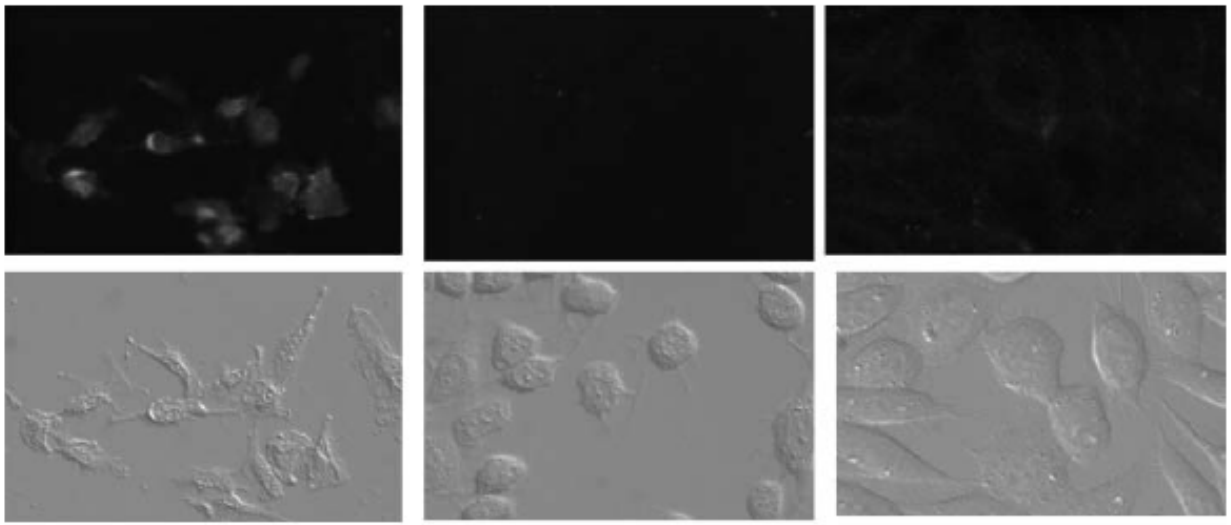

Fig. 1. Imaging CHO cells with Ang II–quantum dot conjugates. The upper panels show the fluorescence images, and the lower panels show the bright-field images. Cells are clearly visible in all of the bright-field images; however, only the cells incubated with Ang II conjugates that express the AT1 receptor are seen to be fluorescent (top left panel). When these cells were preincubated with a 100 μM solution of Ang II, the binding of Ang II-conjugated quantum dots was blocked (top center panel). Finally, when parental cells that did not express the receptor were incubated with the conjugate, no fluorescence was observed (top right panel).

Ang II Q-dot and Alexa-488

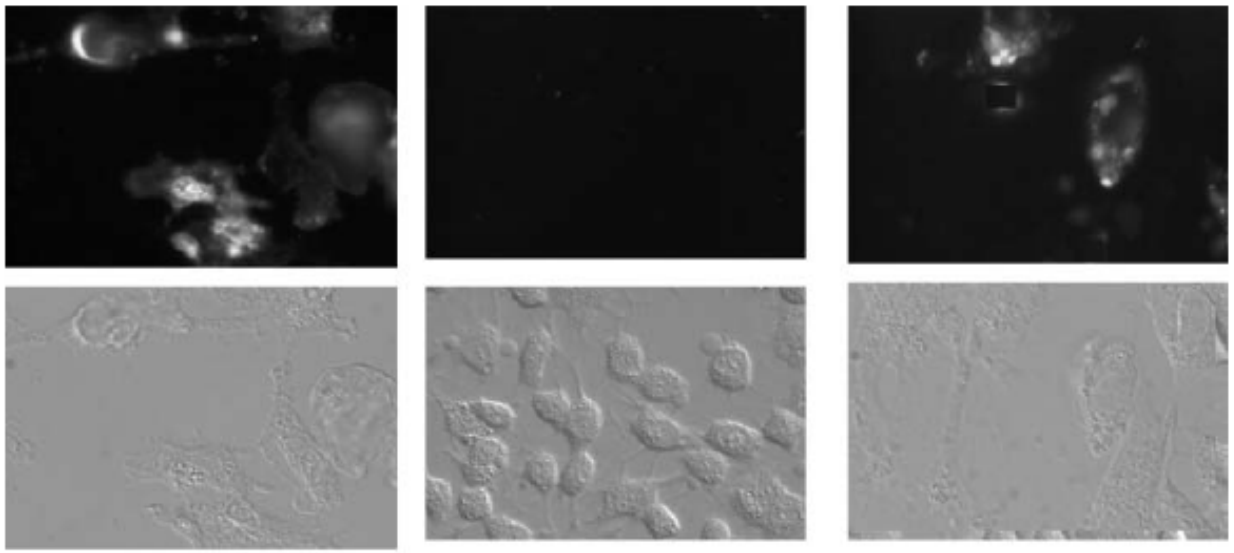

Fig. 2. Imaging CHO cells expressing AT1 receptor using Ang II–quantum dot conjugates and Ang II–Alexa 488. The upper panels show the fluorescent images, and the lower panels show the bright-field images. Cells are clearly visible in all of the bright field images. Cells expressing the AT1 receptor specifically bind Ang II–quantum dot conjugates (top left panel). Similar binding was observed when the cells were incubated with Ang II–Alexa 488 (top right panel). This specific binding of Ang II–quantum dot conjugates was blocked by preincubation of AT1-expressing cells with a 100-μM solution of Ang II (top center panel).

Quantum Dot-Encoded Beads

Xiaohu Gao and Shuming Nie

Multiplexing for high throughput screening

Multiple color + multiple intensity

6 color, 10 intensity = 10 x 10 x 10 x 10 x 10 x 10 = 10^6 coding

Carrier : polystyrene nanobeads,
polystyrene microbeads, mesoporous silica microbeads

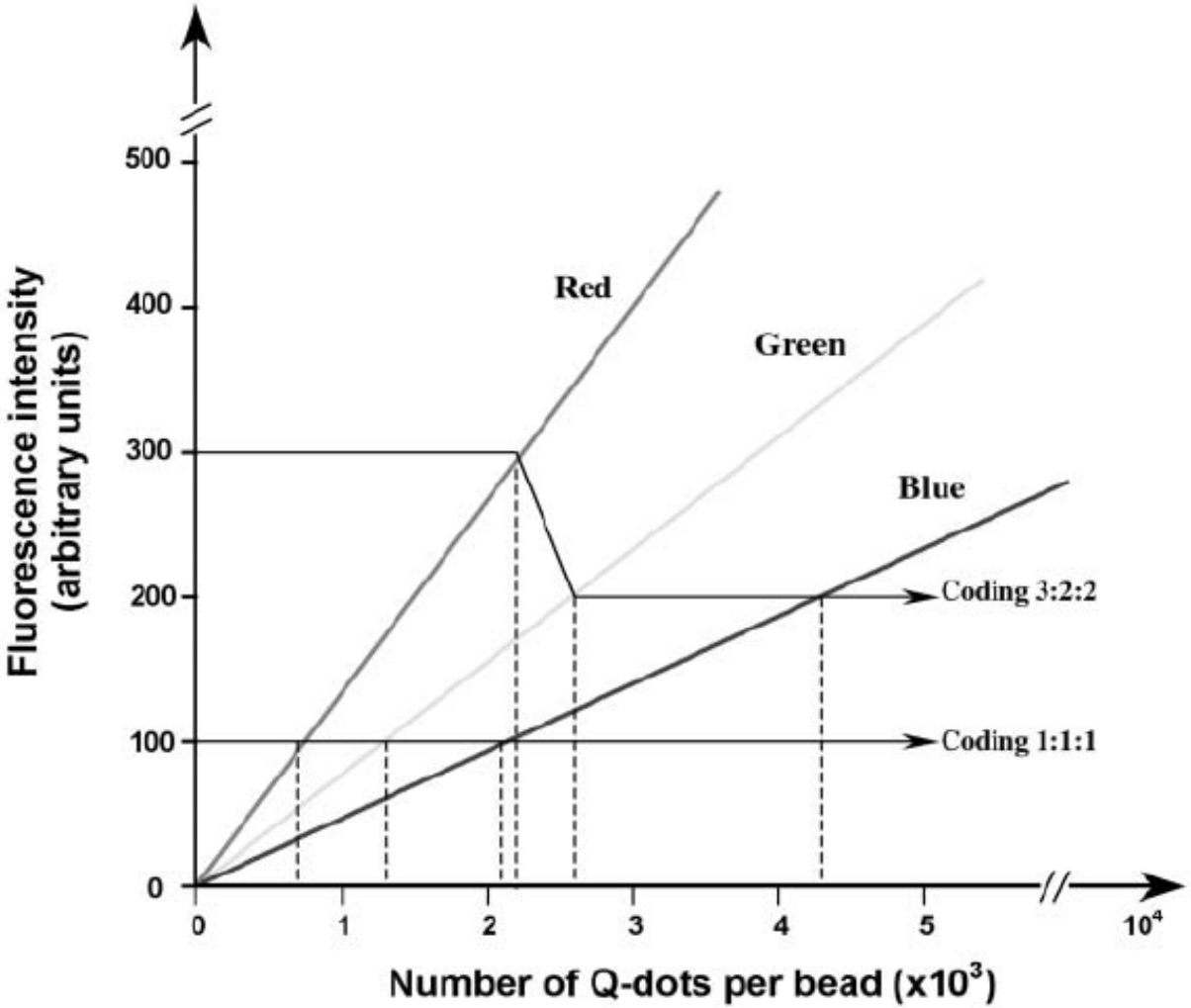

Fig. 1. Schematic drawing of working curves for preparation of multicolor quantum dot microbeads. Arrows depict two representative beads coded with intensity ratios of 1 : 1 : 1 and 3 : 2 : 2, and the number of quantum dots (or concentration) can be obtained from the x axis. Each single bead may contain quantum dots (Q-dots) ranging from several hundred to millions, depending on the bead size and surface area.

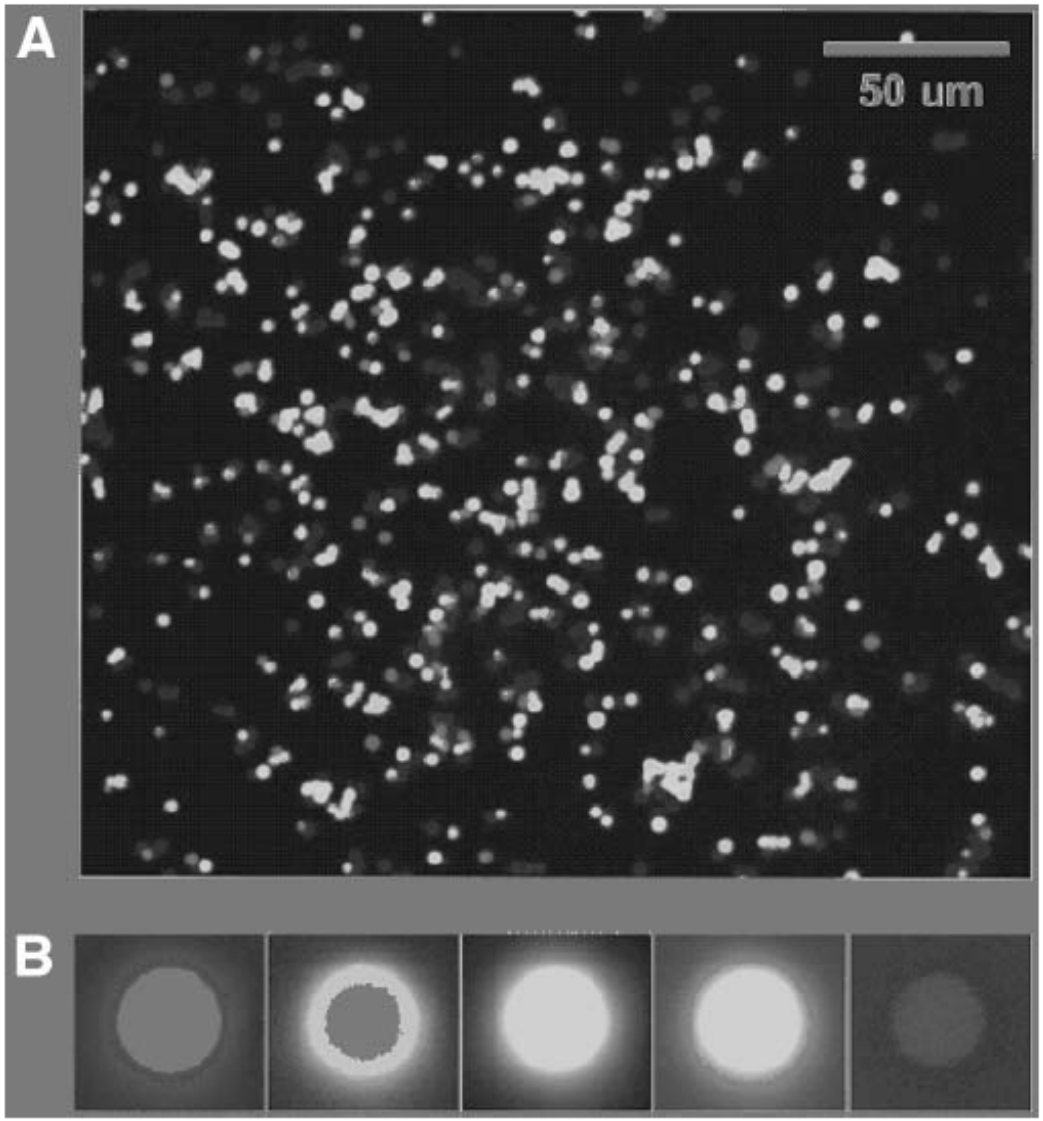

Fig. 2. Fluorescence images of mesoporous silica beads (5-µm diameter, 32-nm pore size) doped with single-color quantum dots emitting light at 488 nm, 520 nm, 550 nm, 580 nm, or 610 nm. **(A)** Wide-field view of large population of doped beads, prepared in batches and then mixed; **(B)** enlarged views of single monochromatic beads. Each bead contains up to 2 million dots of the same color.

Setup

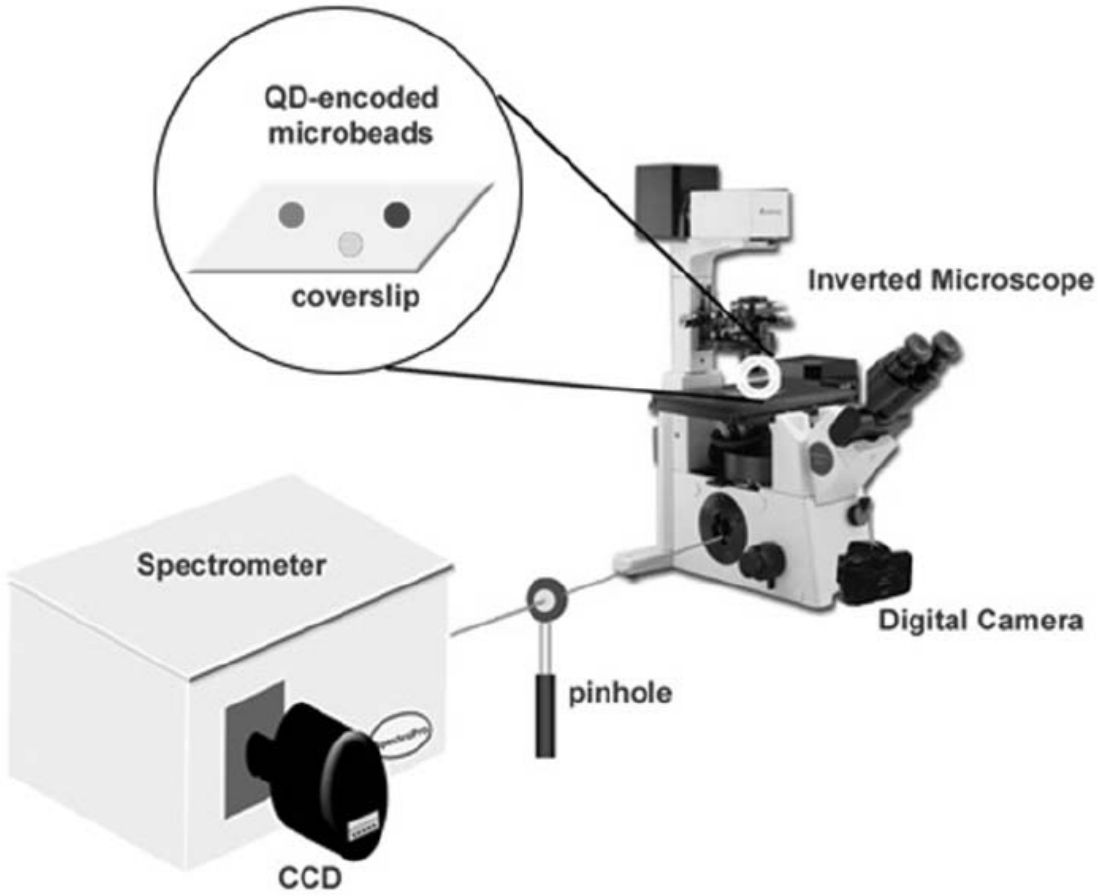

Fig. 3. Schematic diagram of integrated fluorescence imaging and spectroscopy system. The coding signals are read out by a CCD camera and a single-stage spectrometer attached to the side port of an inverted microscope.

Gold Nanoparticles

- Pregnancy test (40 nm gold nanoparticles)
- High extinction coefficient 2×10^9 ($\text{fluorescein } 7 \times 10^4$)
- Easy to modify through thiol chemistry
- Size dependent extinction peaks

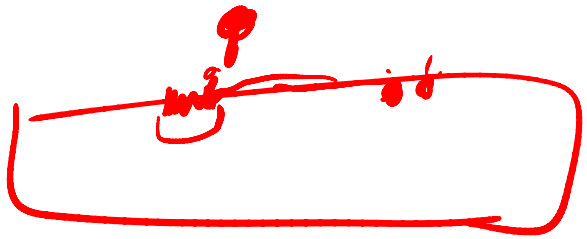

FRET

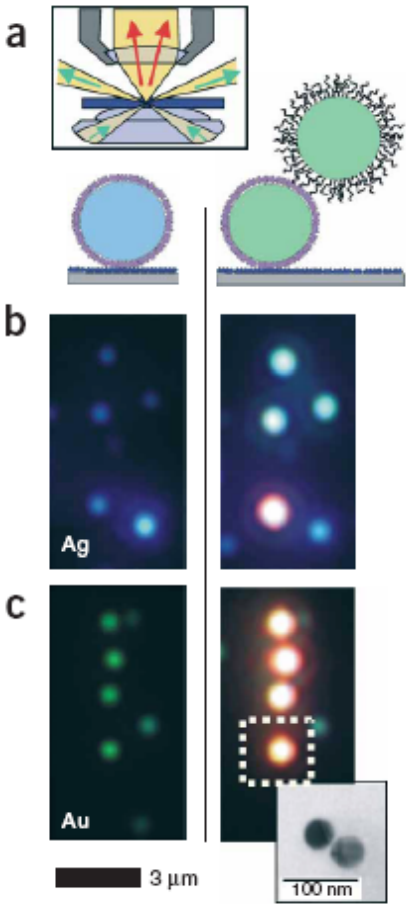

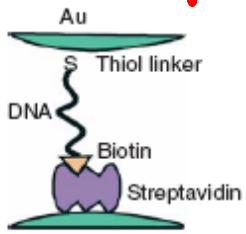

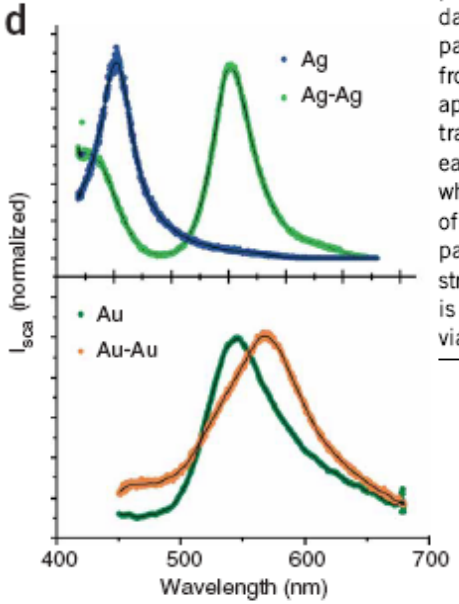

Figure 1 Color effect on directed assembly of DNA-functionalized gold and silver nanoparticles. (**a**) First, nanoparticles functionalized with streptavidin are attached to the glass surface coated with BSA-biotin (left). Then, a second particle is attached to the first particle (center), again via biotin-streptavidin binding (right). The biotin on the second particle is covalently linked to the 3′ end of a 33 base pair long ssDNA strand bound to the particle via a thiol group at the 5′ end. Inset: principle of transmission darkfield microscopy. (**b**) Single silver particles appear blue (left) and particle pairs blue-green (right). The orange dot in the bottom comes from an aggregate of more than two particles. (**c**) Single gold particles appear green (left), gold particle pairs, orange (right). Inset: representative transmission electron microscopy image of a particle pair to show that each colored dot comes from light scatted from two closely lying particles, which cannot be separated optically. (**d**) Representative scattering spectra of single particles and particle pairs for silver (top) and gold (bottom). Silver particles show a larger spectral shift (102 nm) than gold particles (23 nm), stronger light scattering and a smaller plasmon line width. Gold, however, is chemically more stable and is more easily conjugated to biomolecules via –SH, –NH2 or –CN functional groups.

2nm – 70 nm

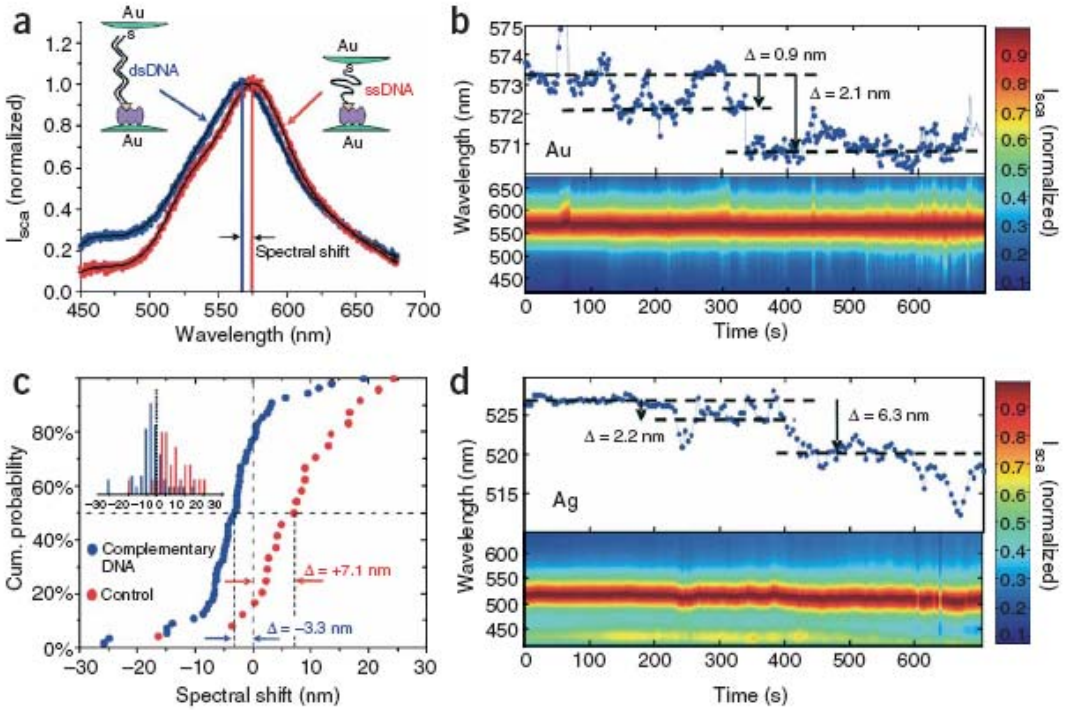

Figure 3 Spectral shift upon DNA hybridization. (**a**) Example of a spectral shift between a gold particle pair connected with ssDNA (red) and dsDNA (blue). The shift is clearly visible. (**b**) Spectral position as a function of time after addition of complementary DNA. The scattered intensity (Isca) is shown color-coded on the bottom; the peak position obtained by fitting each spectrum is traced on the top. Discrete states are observed, indicated by horizontal dashed lines. (**c**) Cumulative probability distribution of the spectral shift for ~80 particles induced by adding complementary DNA (blue) and noncomplementary DNA (red). Inset: histogram of the observed spectral shift. A student's *t*-test on this data proves the difference between experiment and control to be statistically significant ($P < 0.0001$). (**d**) Time dynamics for a silver particle dimer after addition of complementary DNA. The random fluctuations in the time traces due to solution effects and Brownian motion could be used to gain insight into the interparticle potential.

Gold Surface Modification

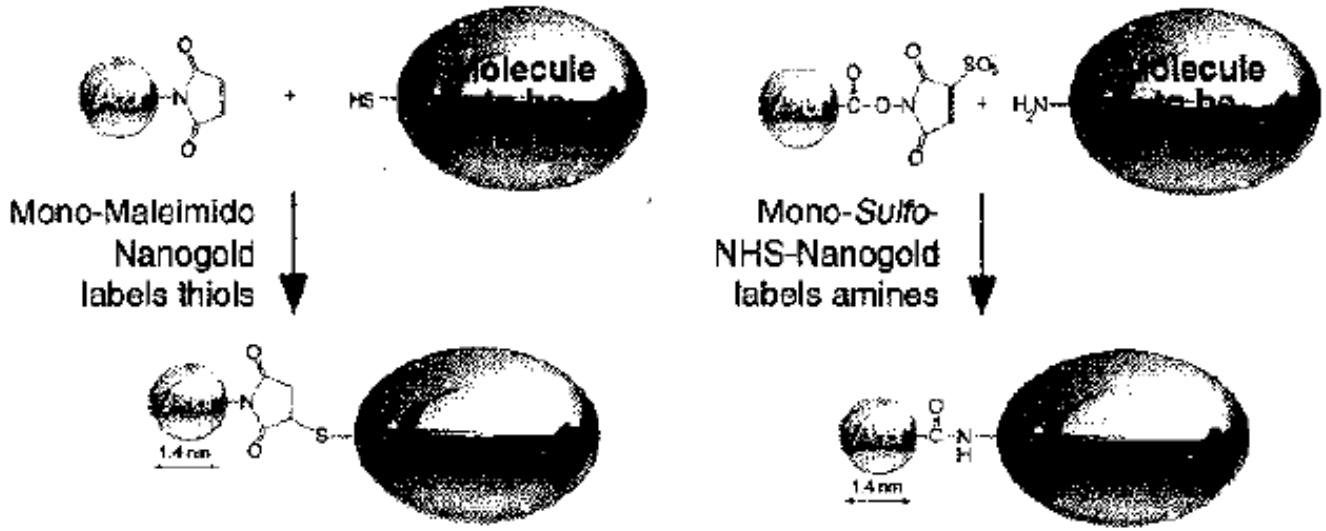

Figure 23.1 Schematic showing reactions of Mono-Maleimido-Nanogold and Mono-*Sulfo*-NHS-Nanogold.

Au9 . Au13 . Au1

SAM for Surface Modification

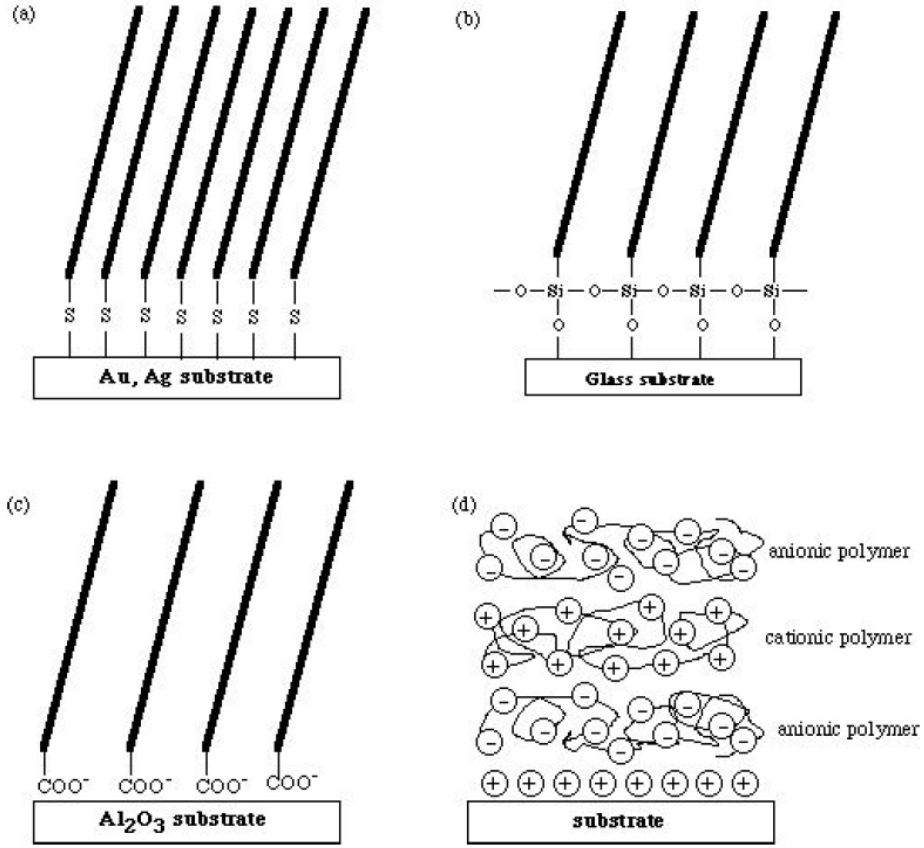

Fig. 1 Model of the surfaces of various SAMs

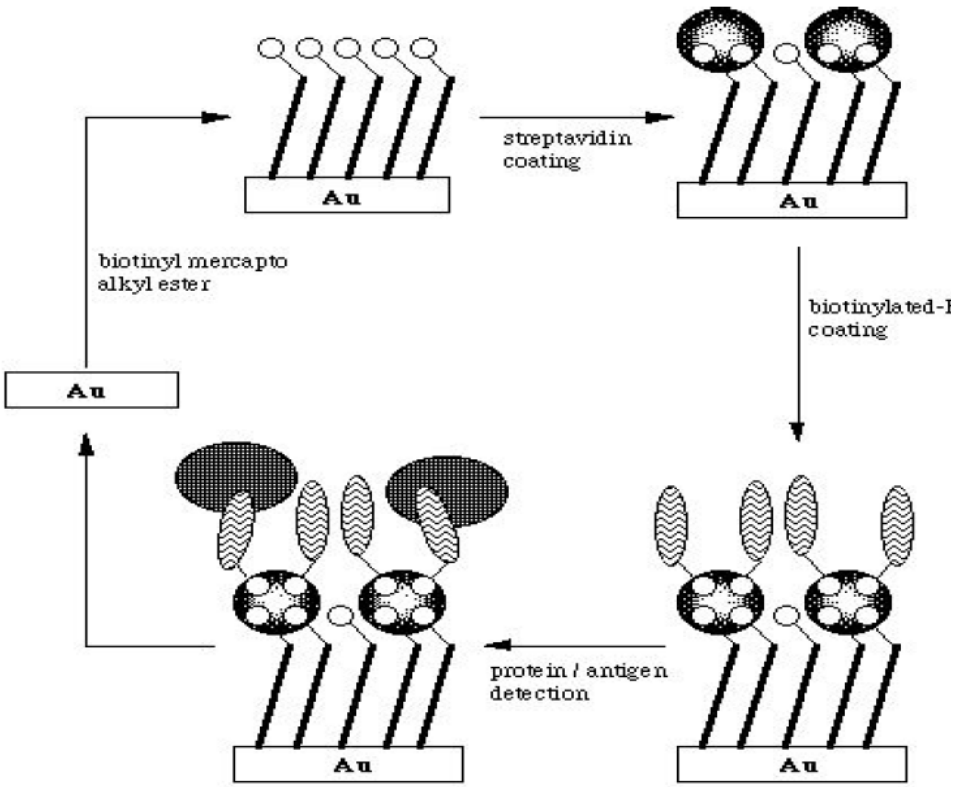

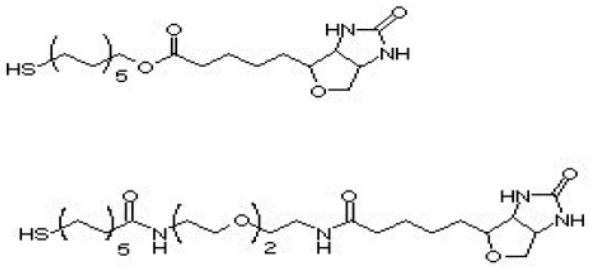

biotin-ω-mercapto alkyl esters

Fig. 14 Reversible formation of a protein triple layer on SAM using biotinvlated alkvlthiols.

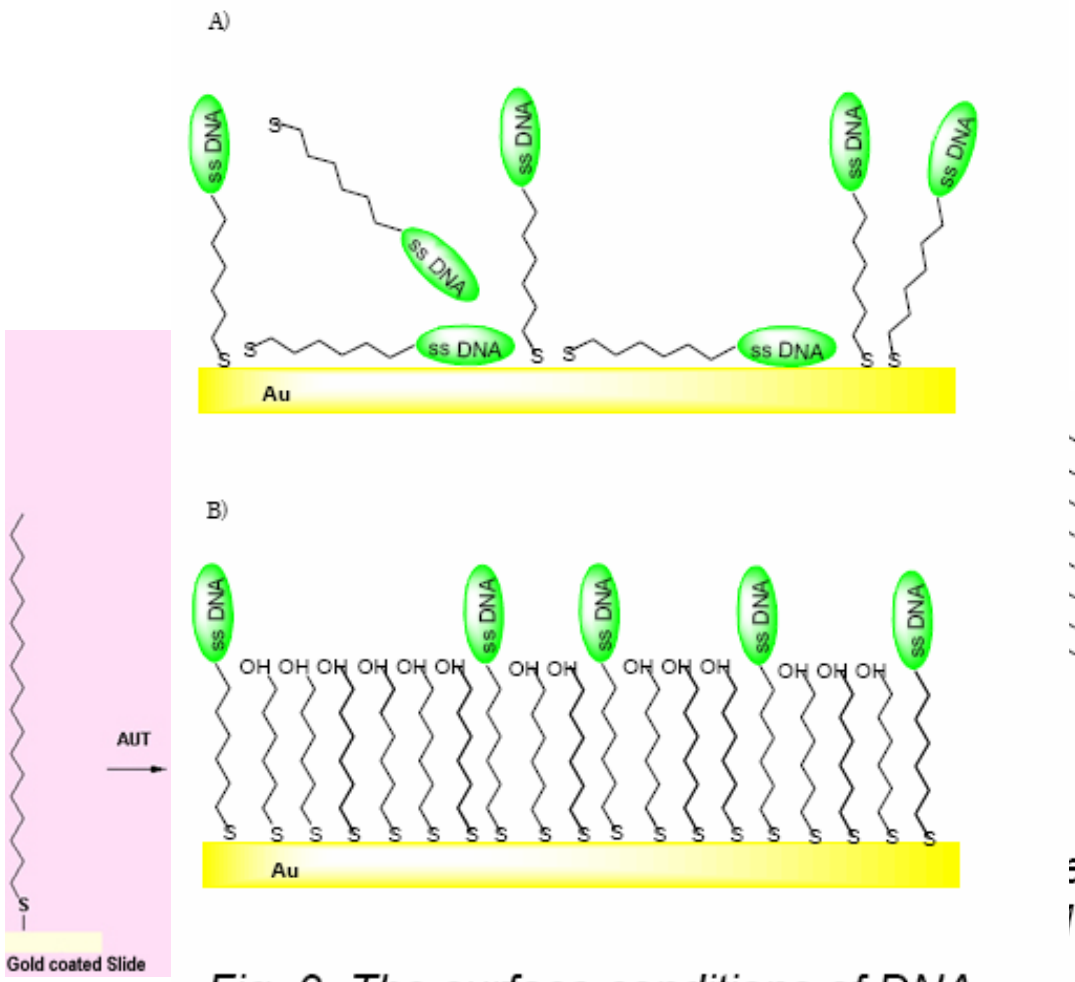

Fig. 9 The surface conditions of DNA sensor
A) HS-ss-DNA only
B) Coexistence of HS-ss-DNA and 6-hydroxy-1-hexanethiol

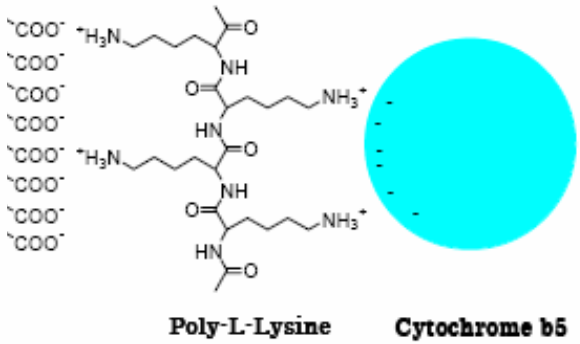

e structure cytochrome b5/
l gold immobilized ultilayer

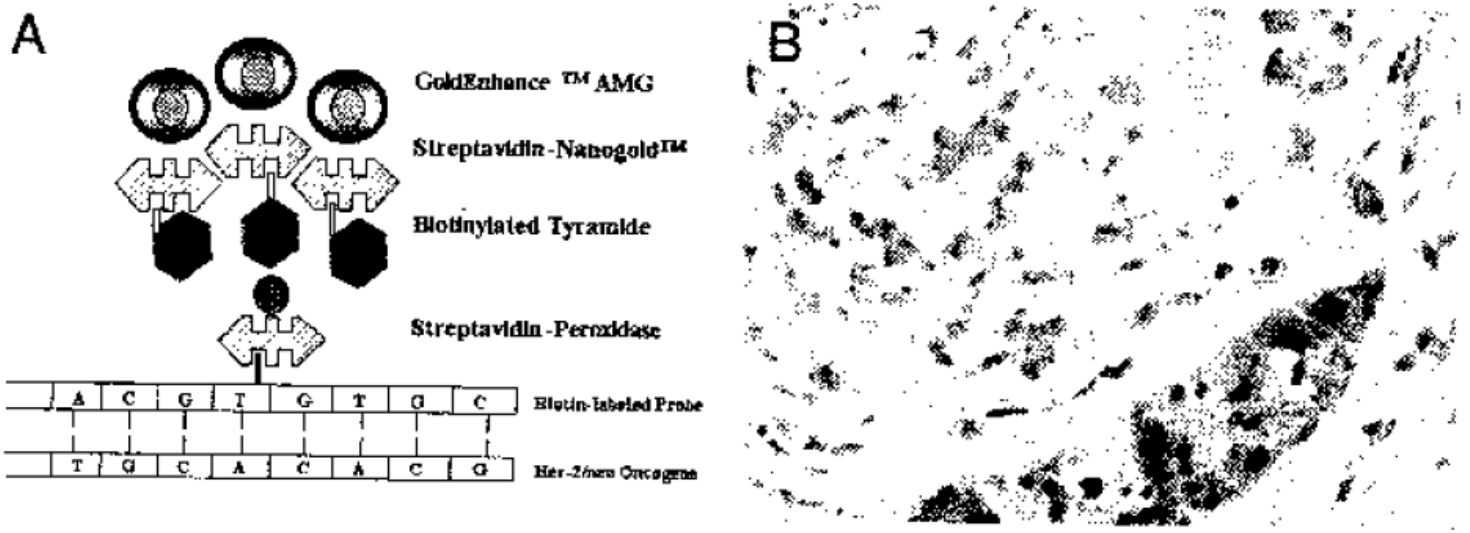

Figure 23.6 (A) Final configuration for GOLDFISH in-situ hybridization assay. (B) A non-neoplastic duct displaying normal endogenous (nonamplified) HER-2/neu gene copy (left) is surrounded by infiltrating duct carcinoma demonstrating HER-2/neu gene amplification (right). GOLDFISH with nuclear fast red counterstains; original magnification, ×400. (From Ref. [107].)

Assembly and Characterization of Biomolecule–Gold Nanoparticle Conjugates and Their Use in Intracellular Imaging

Alexander Tkachenko, Huan Xie, Stefan Franzen, and Daniel L. Feldheim

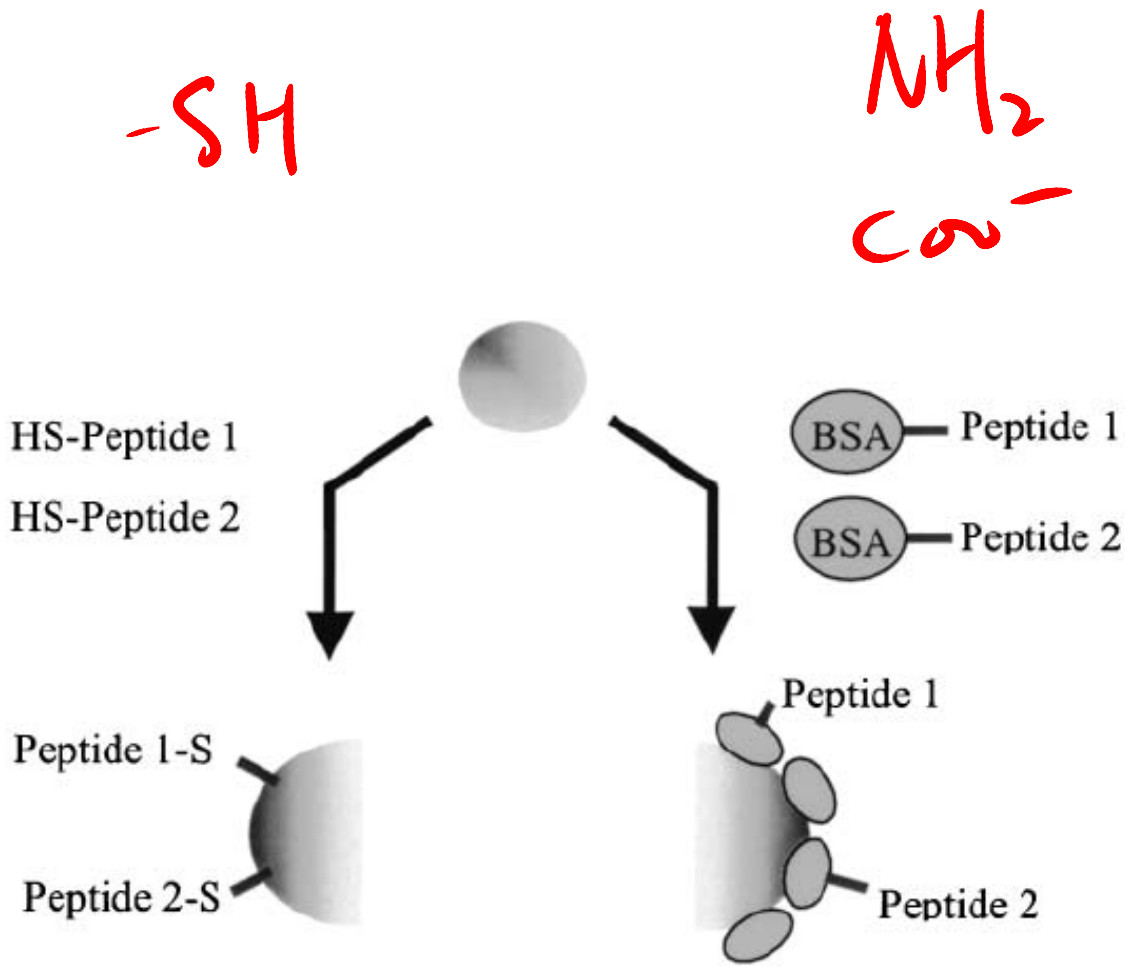

Fig. 1. Two strategies for assembling multifunctional gold particle–peptide bioconjugates.

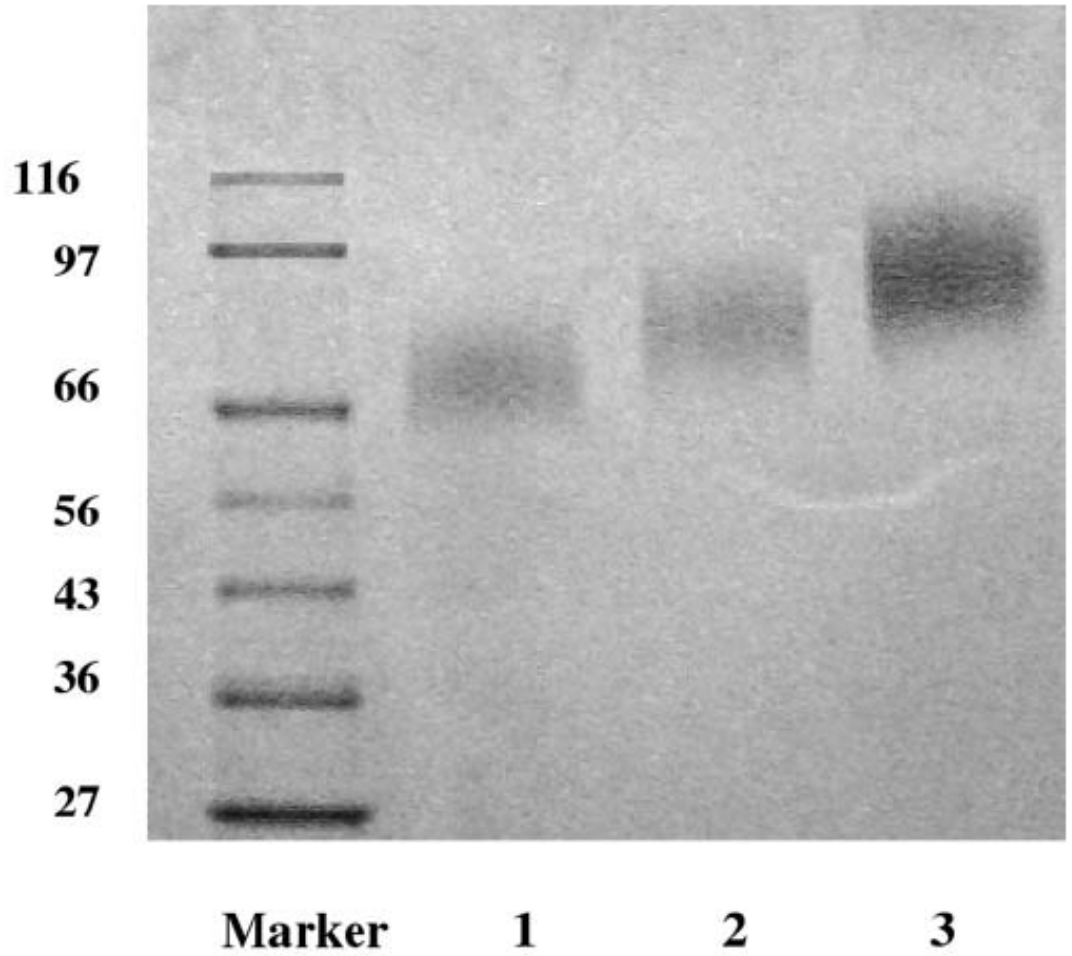

Fig. 2. Gel shift assay, 7.5%, SDS-PAGE gel: lane 1, BSA/MBS complex at 1:40 ratio; lane 2, BSA/peptide at 1:3 ± 1 ratio; lane 3, BSA/peptide at 1:6 ± 2 ratio. The broad nature of the sample bands reflects various binding efficiencies within the sample. Marker bands correspond to the molecular weight in thousands on the left.

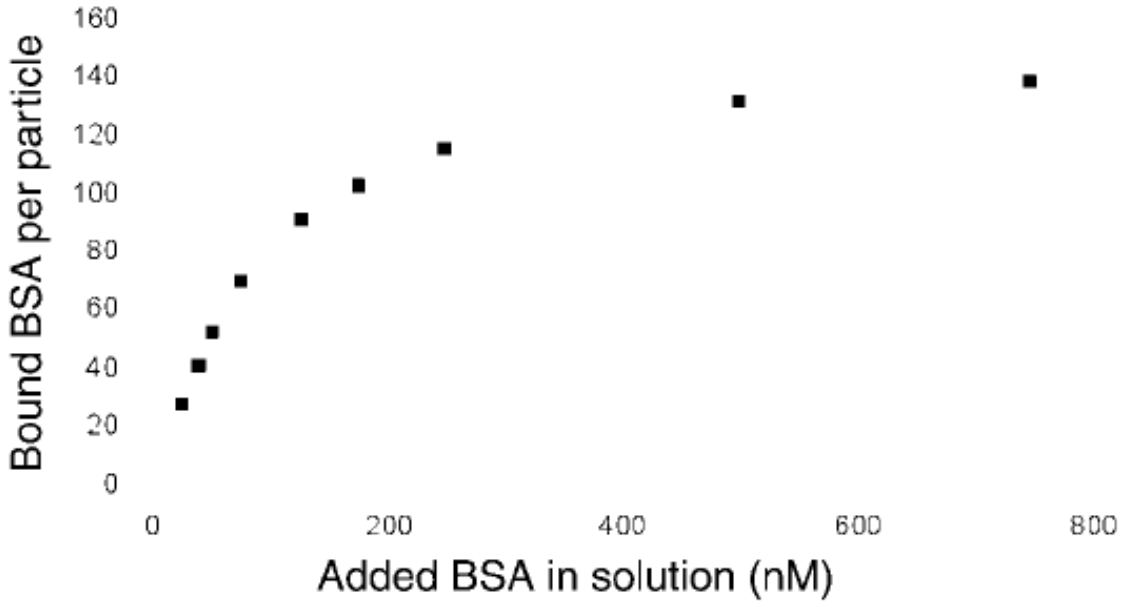

Fig. 3. Adsorption isotherm of RBITC-labeled BSA adsorbed on gold particles (20 nm in diameter).

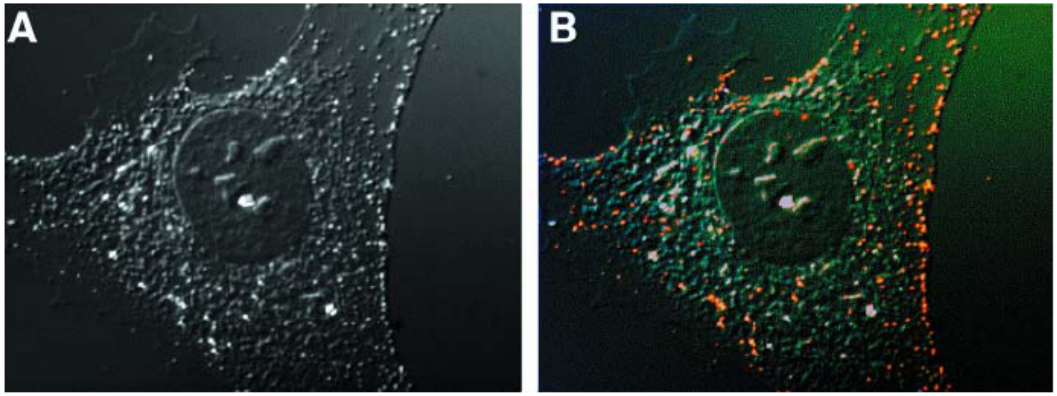

Fig. 4. Comparison of **(A)** video-enhanced black-and-white DIC microscopy and **(B)** video-enhanced color DIC microscopy. Shown are 20-nm-diameter gold-peptide-BSA complexes inside 3T3 cells. Images were taken with a Nikon DXM 1200 digital color CCD camera on a Leica DMLB DIC-equipped microscope with a ×100/1.3 NA objective.

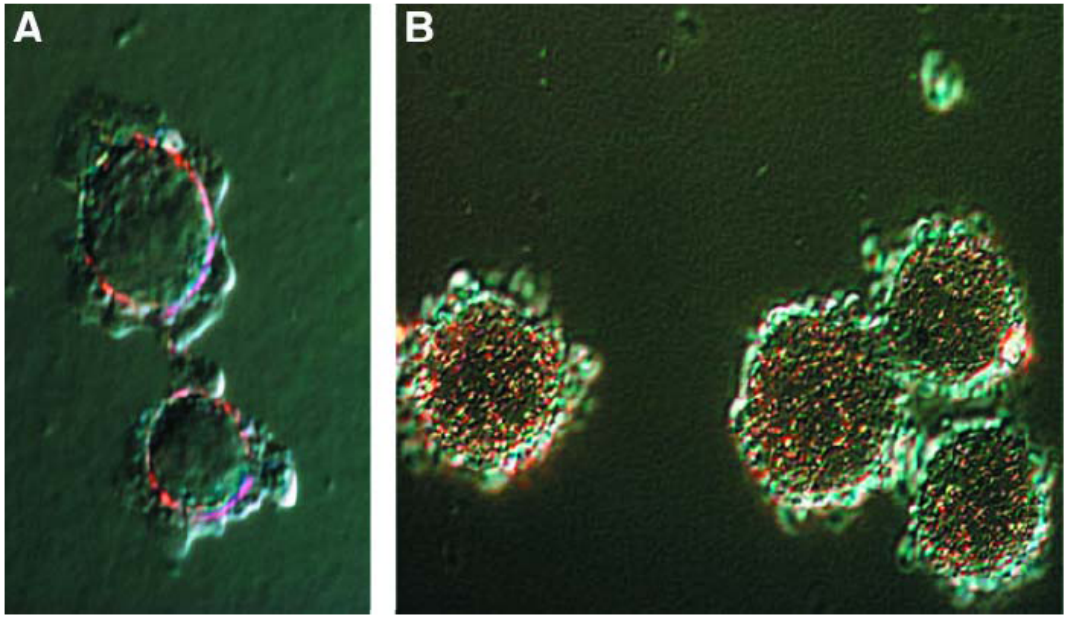

Fig. 5. Incubation of HeLa cells with 20-nm gold nanoparticles after 3 h by VECDIC microscopy. **(A)** Nanoparticle carrying Large T NLS accumulated around nuclear membrane. **(B)** Nanoparticle carrying adenovirus NLS accumulated inside nucleus.

Use of Nanobarcodes® Particles in Bioassays

R. Griffith Freeman, Paul A. Raju, Scott M. Norton,
Ian D. Walton, Patrick C. Smith, Lin He, Michael J. Natan,
Michael Y. Sha, and Sharron G. Penn

Submicrometer Metallic Barcodes

Sheila R. Nicewarner-Peña,[1] R. Griffith Freeman,[2]
Brian D. Reiss,[1] Lin He,[2] David J. Peña,[1] Ian D. Walton,[2]
Remy Cromer,[2] Christine D. Keating,[1]* Michael J. Natan[2]*

SCIENCE VOL 294 5 OCTOBER 2001

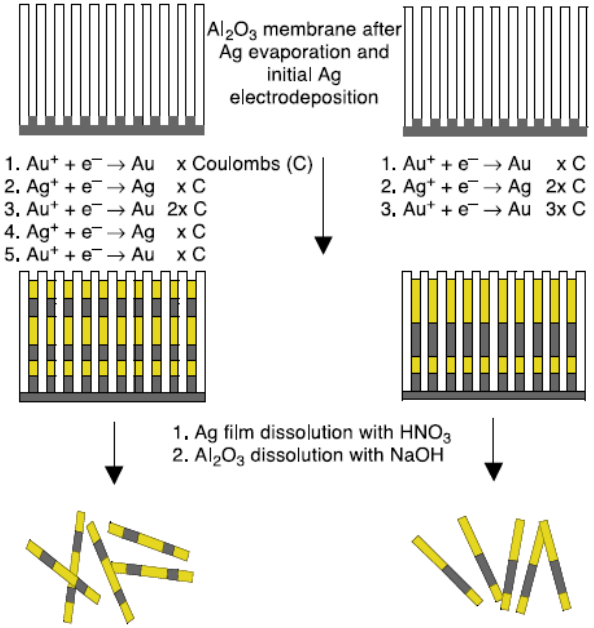

Fig. 1. Synthesis of barcoded particles.

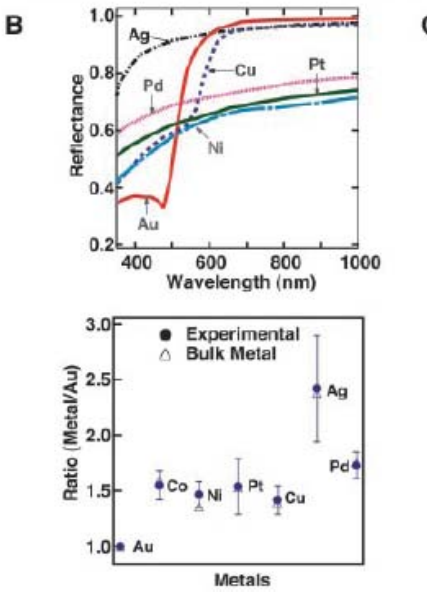

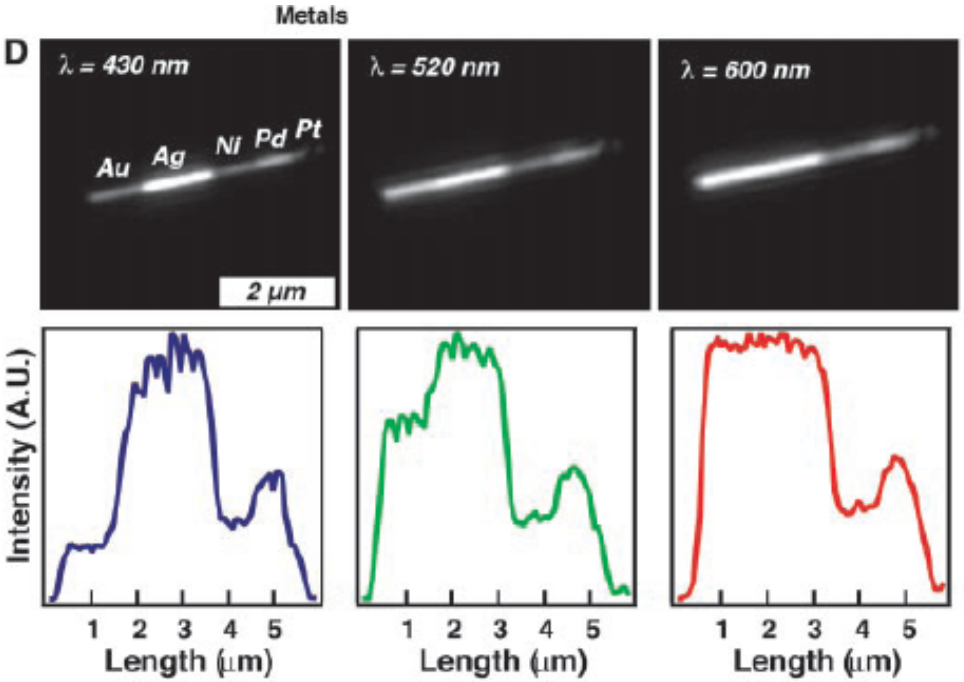

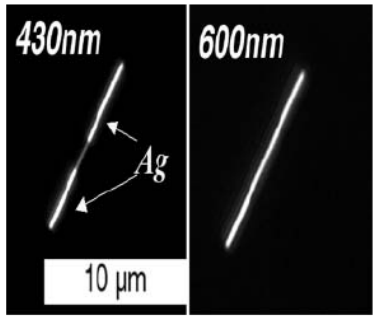

Fig. 1. Differences in reflectivity at 430 vs 600 nm for NBC sequence Ag-Au-Ag.

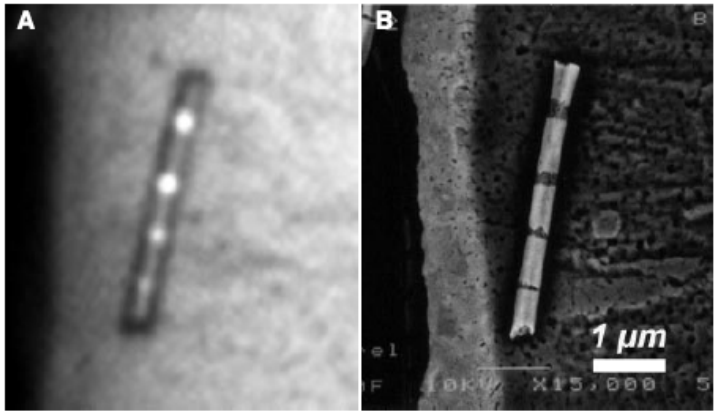

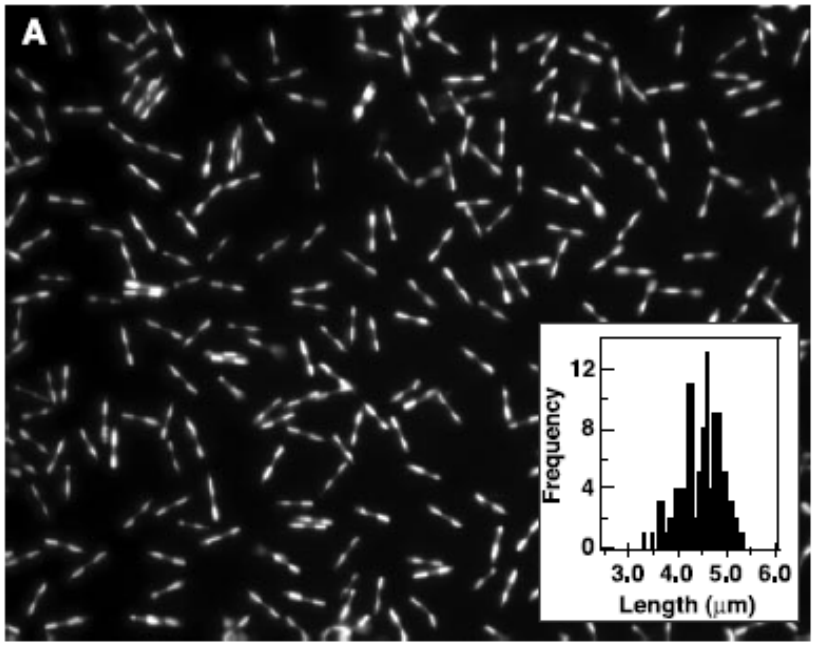

Surface Functionalization

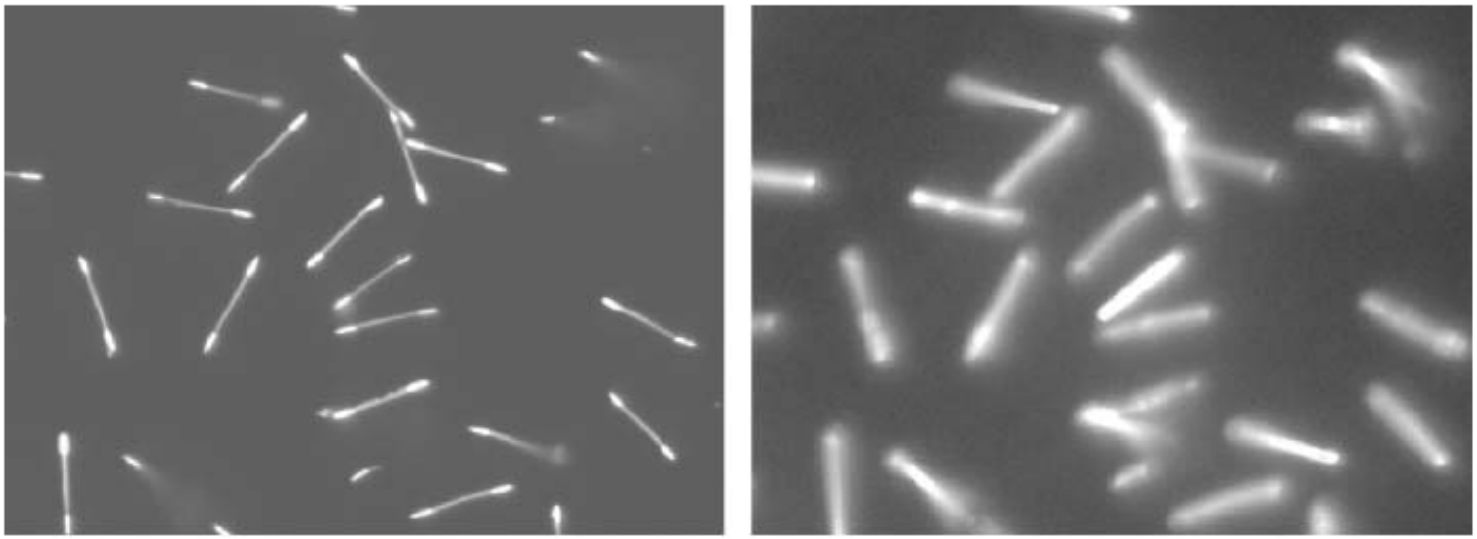

Reflectance **Fluorescence**

Fig. 2. Signal detection of oligonucleotide-derivatized NBCs hybridized with complementary Cy5 oligonucleotide.

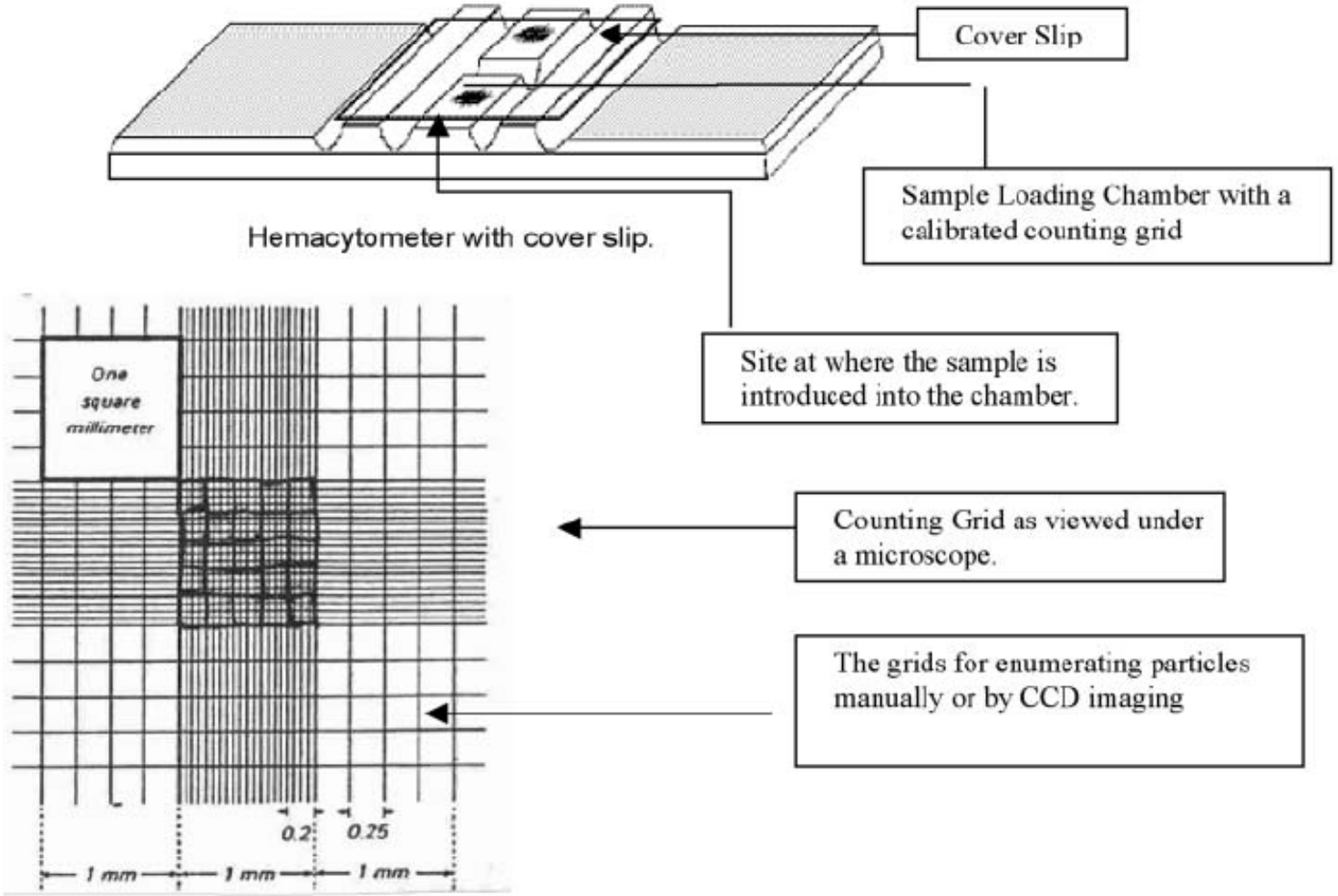

Fig. 3. Layout of hemacytometer.

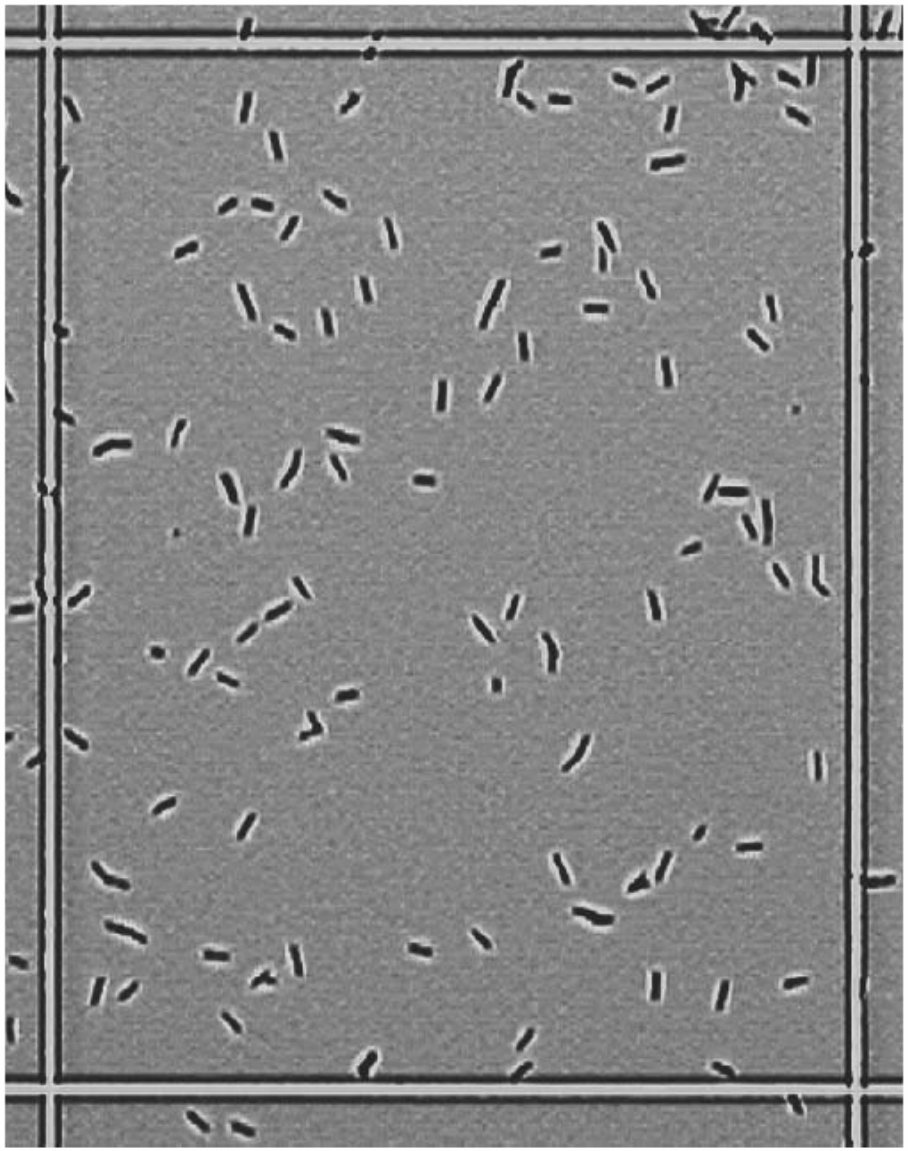

Fig. 4. NBC particles as they appear in 1 of the 16 grids (4×4 squares grid) using a $\times 20$ objective lens in a hemacytometer.

Whole-Blood Immunoassay Facilitated by Gold Nanoshell–Conjugate Antibodies

Lee R. Hirsch, Naomi J. Halas, and Jennifer L. West

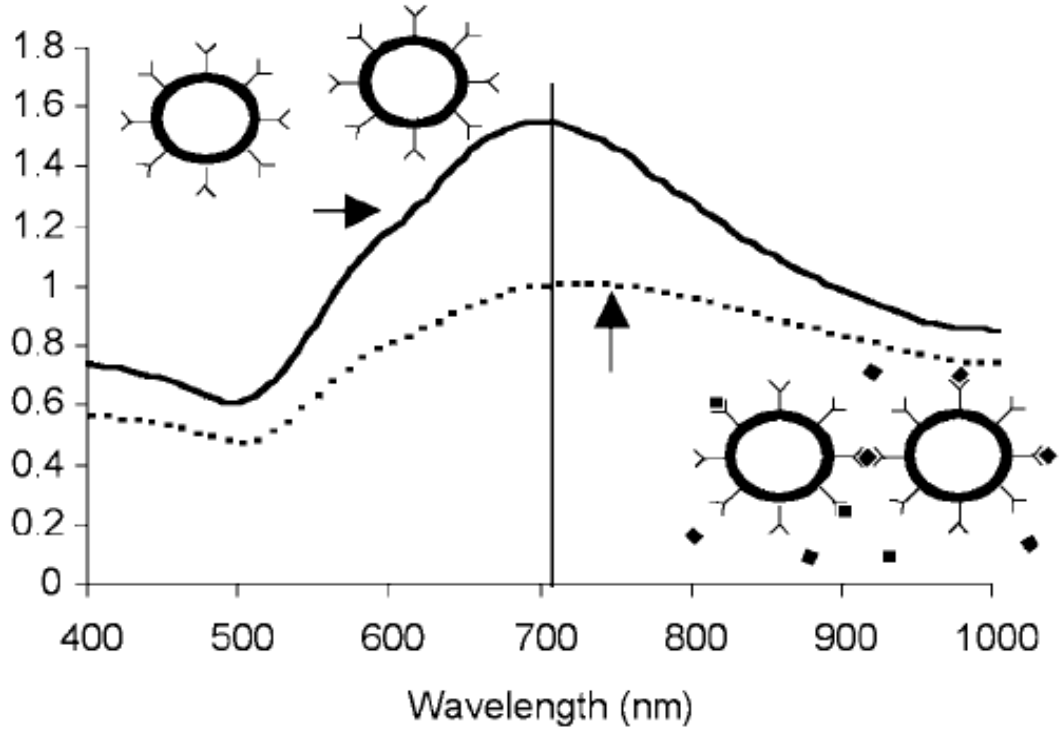

Fig. 1. Well-dispersed antibody-nanoshell conjugates in the absence of analyte possess a well-defined extinction peak in the near-IR. In the presence of the complementary analyte, multiple nanoshells bind to the analyte, causing agglutination and a corresponding reduction in the extinction peak.

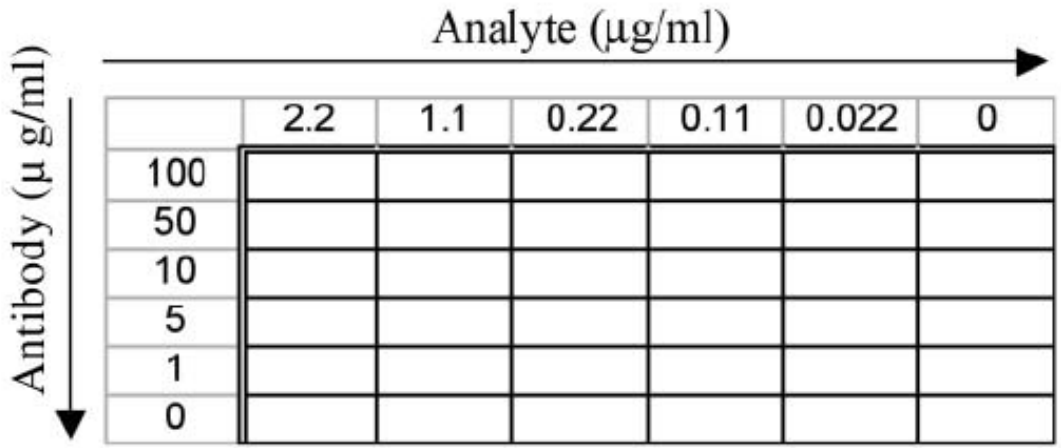

Fig. 2. Diagram of 2D matrix for determining optimal antibody and analyte concentration for maximal agglutination.

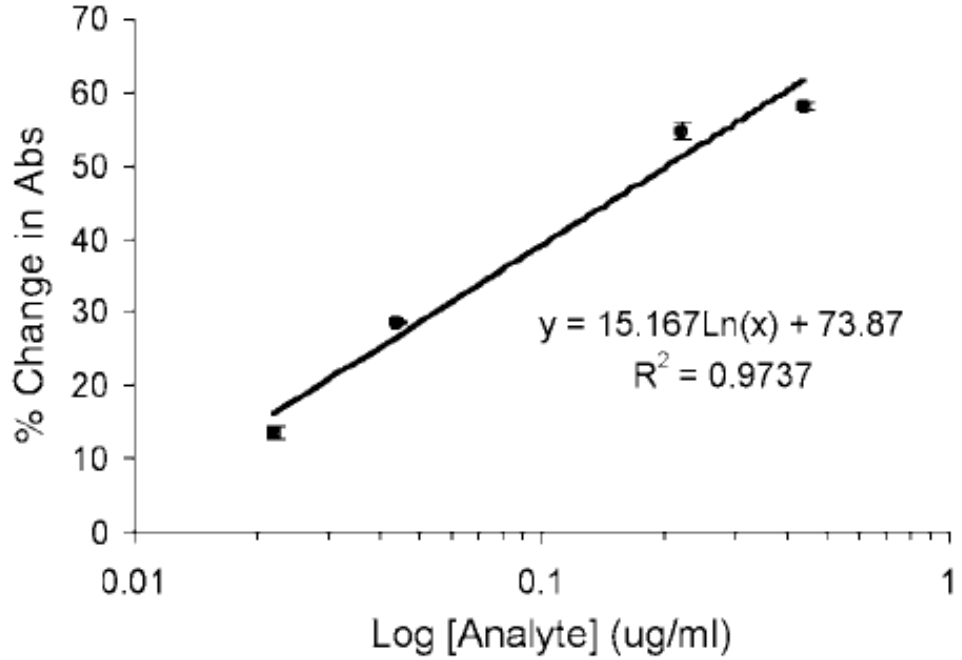

Fig. 3. Standard curve depicting log-linear behavior of antibody-nanoshell agglutination in presence of analyte.

Surface-Functionalized Nanoparticles for Controlled Drug Delivery

Sung-Wook Choi, Woo-Sik Kim, and Jung-Hyun Kim

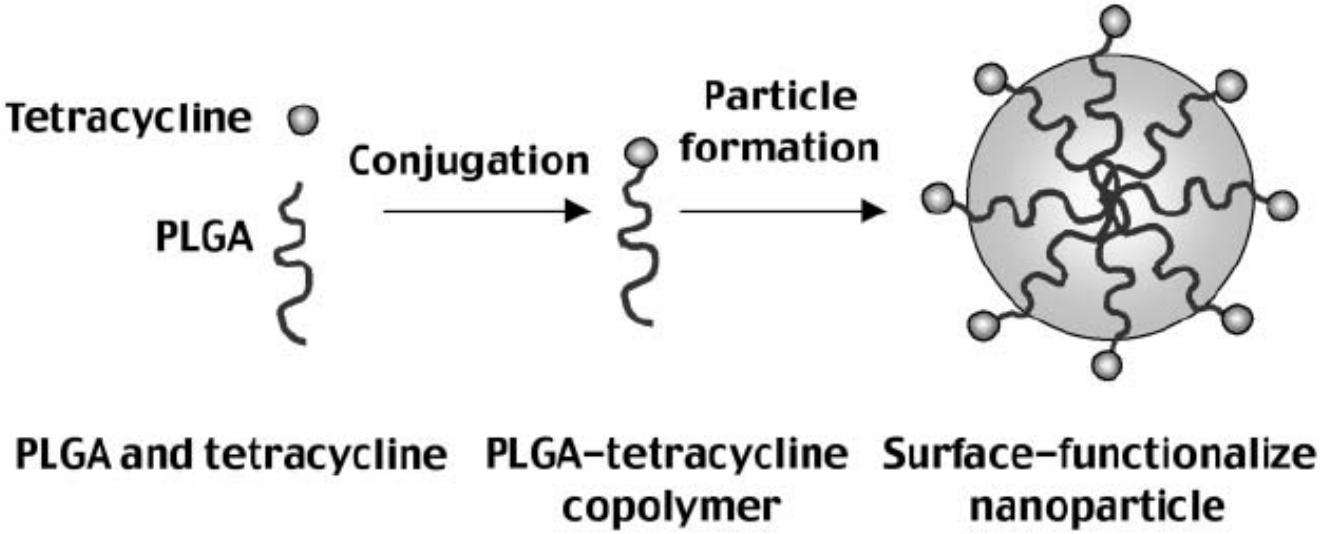

Fig. 1. Overall procedure for preparation of surface-functionalized nanoparticle.

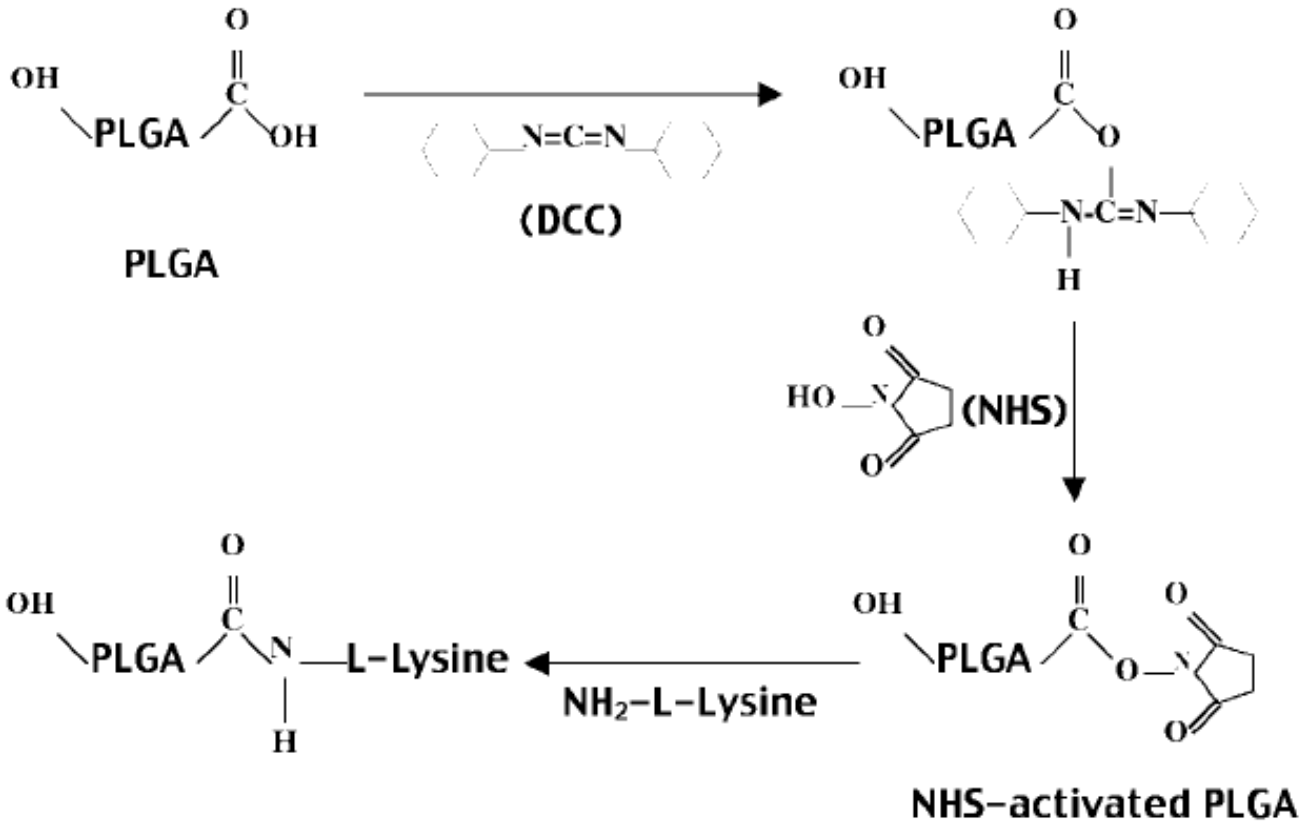

Fig. 2. Schematic diagram of conjugation of PLGA-tetracycline copolymer.

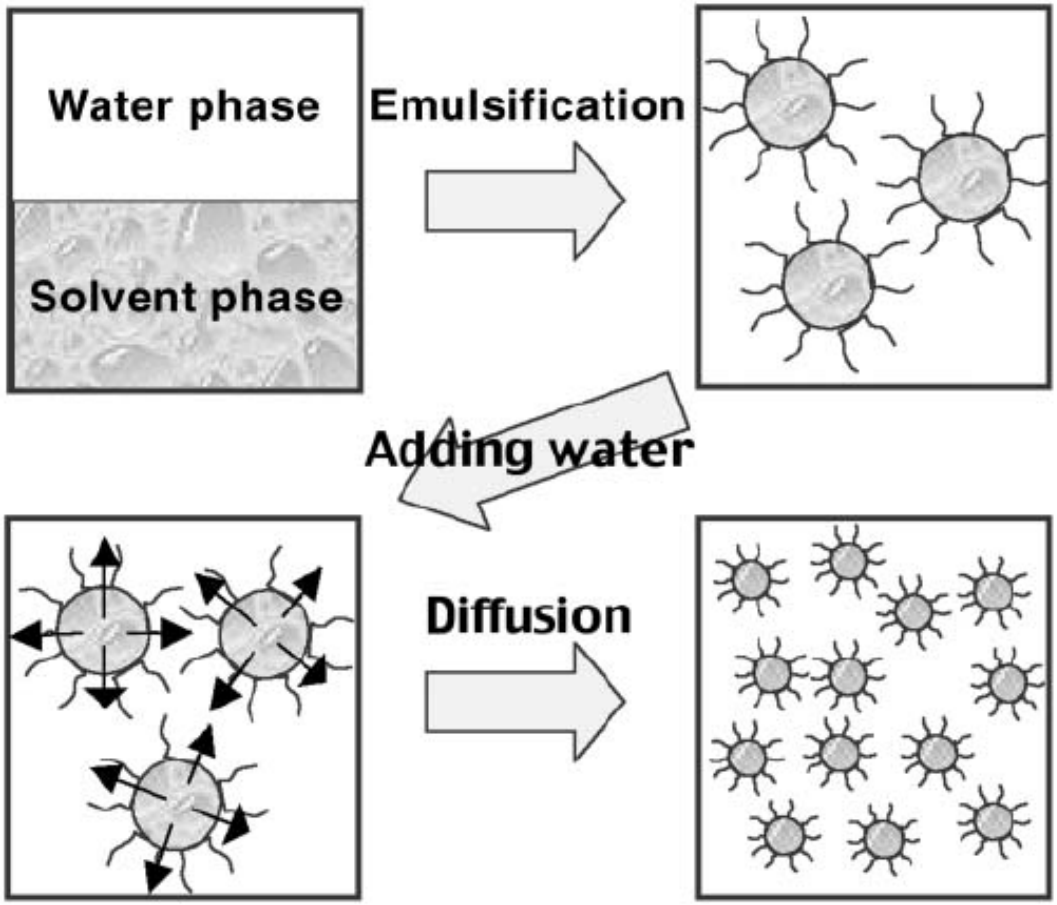

Fig. 3. Nanoparticle preparation by emulsification-diffusion method.

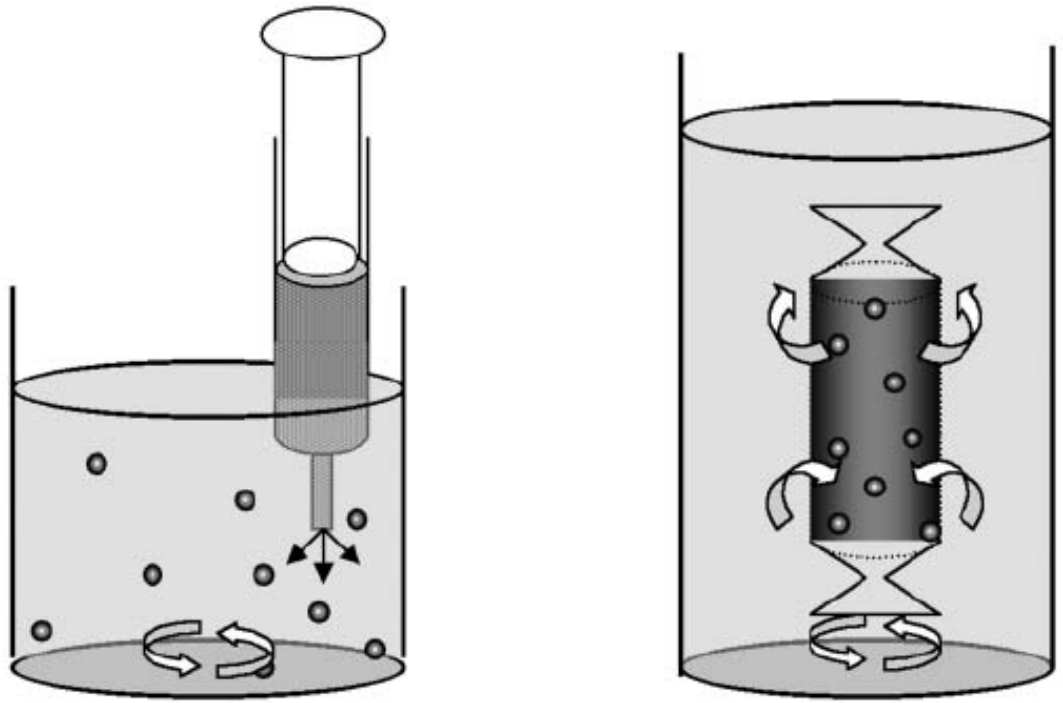

Fig. 4. Schematic illustration of nanoprecipitation (**left**) and dialysis method (**right**).

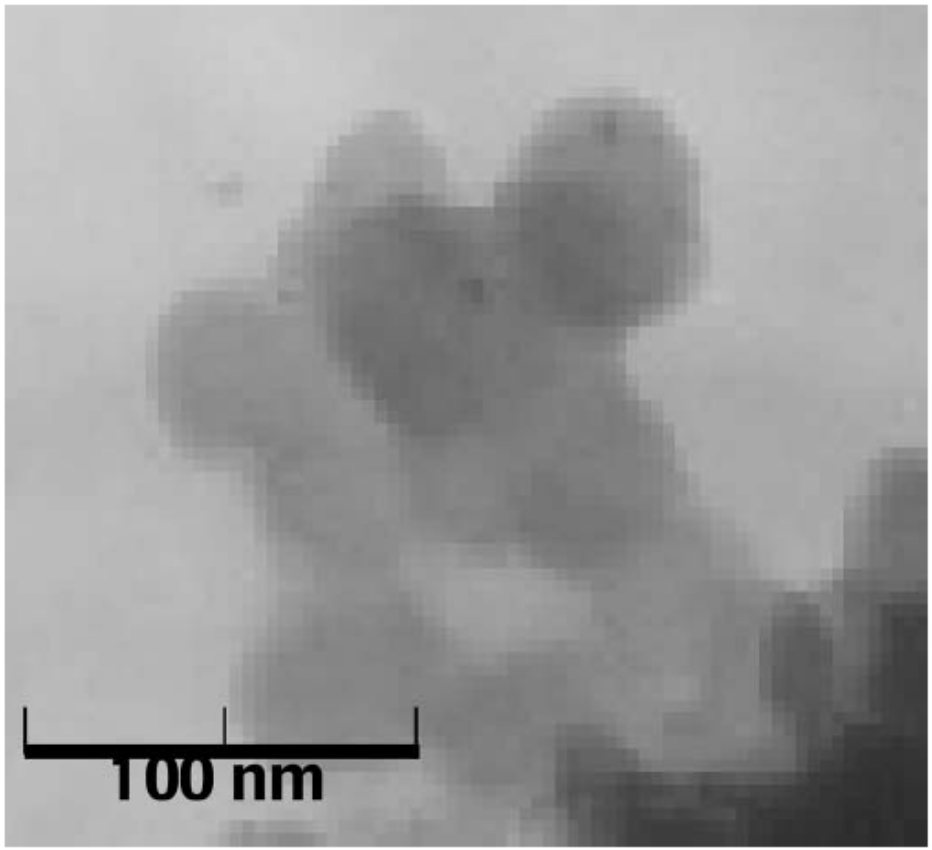

Fig. 5. Transmission electron microscopy image of PLGA nanoparticles prepared by emulsification-diffusion method.

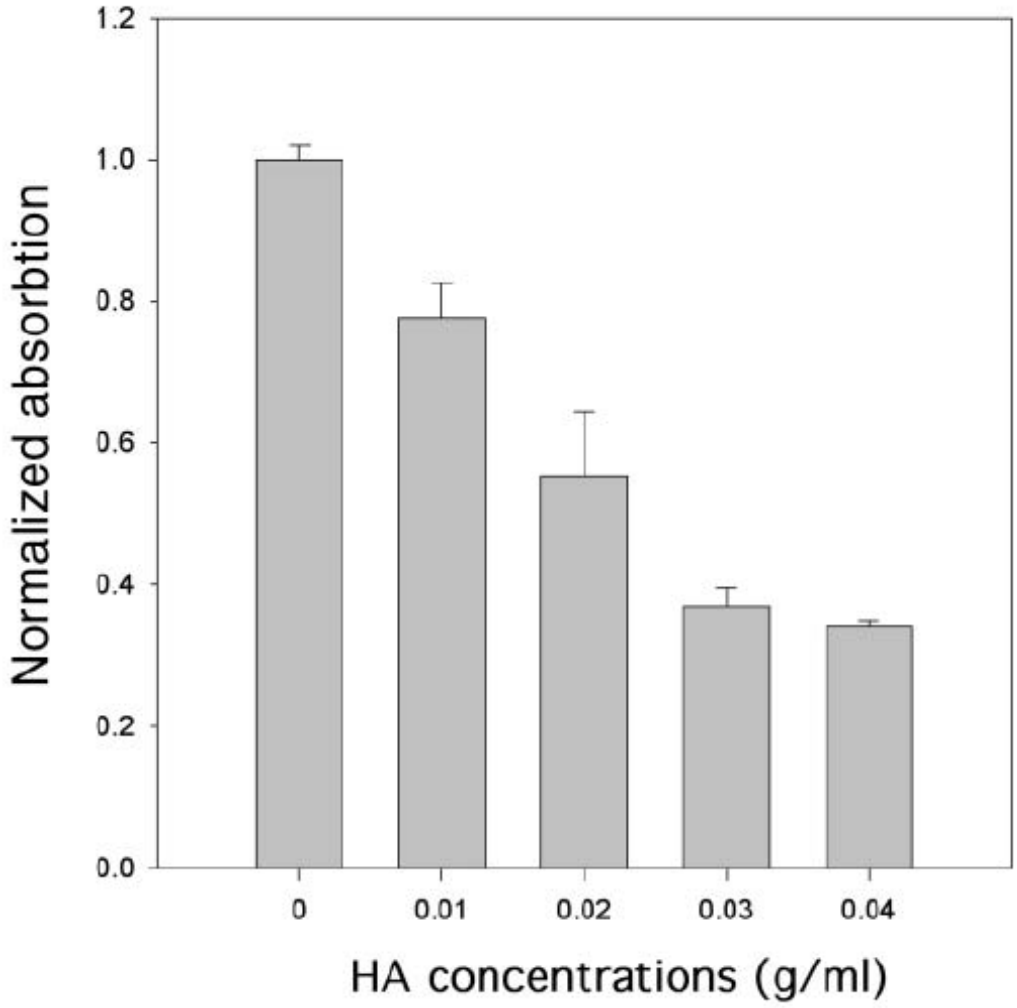

Fig. 6. Affinity of tetracycline-modified nanoparticles on HA.